Analytica Chimica Acta 673 (2010) 1–25

Contents lists available at ScienceDirect

Analytica Chimica Acta

journal homepage: www.elsevier.com/locate/aca

Review

Beyond labels: A review of the application of quantum dots as integrated components of assays, bioprobes, and biosensors utilizing optical transduction

W. Russ Algar, Anthony J. Tavares, Ulrich J. Krull*

Chemical Sensors Group, Department of Chemical and Physical Sciences, University of Toronto Mississauga, Mississauga, Ontario L5L 1C6, Canada

ARTICLE INFO

Article history:
Received 18 February 2010
Received in revised form 17 May 2010
Accepted 17 May 2010
Available online 25 May 2010

Keywords:
Quantum dots
Fluorescence resonance energy transfer
Bioluminescence resonance energy transfer
Electrochemiluminescence
Charge transfer
Immobilization

ABSTRACT

A comprehensive review of the development of assays, bioprobes, and biosensors using quantum dots (QDs) as integrated components is presented. In contrast to a QD that is selectively introduced as a label, an integrated QD is one that is present in a system throughout a bioanalysis, and simultaneously has a role in transduction and as a scaffold for biorecognition. Through a diverse array of coatings and bioconjugation strategies, it is possible to use QDs as a scaffold for biorecognition events. The modulation of QD luminescence provides the opportunity for the transduction of these events via fluorescence resonance energy transfer (FRET), bioluminescence resonance energy transfer (BRET), charge transfer quenching, and electrochemiluminescence (ECL). An overview of the basic concepts and principles underlying the use of QDs with each of these transduction methods is provided, along with many examples of their application in biological sensing. The latter include: the detection of small molecules using enzyme-linked methods, or using aptamers as affinity probes; the detection of proteins via immunoassays or aptamers; nucleic acid hybridization assays; and assays for protease or nuclease activity. Strategies for multiplexed detection are highlighted among these examples. Although the majority of developments to date have been *in vitro*, QD-based methods for *ex vivo* biological sensing are emerging. Some special attention is given to the development of solid-phase assays, which offer certain advantages over their solution-phase counterparts.

Contents

Abbreviations: A647, Alexa Fluor 647; APTES, aminopropyltriethoxysilane; ATP, adenosine triphosphate; Au NPs, gold nanoparticles; β-CD, β-cyclodextrin; BRET, bioluminescence resonance energy transfer; BSA, bovine serum albumin; CB, conduction band; CNTs, carbon nanotubes; ConA, concanavalin A; CRET, chemiluminescence resonance energy transfer; CT, charge transfer; cTnI, human cardiac troponin I; DHLA, dihydrolipoic acid; ECL, electrochemiluminescence; EDTA, ethylenediaminetetraacetic acid; ELISA, enzyme linked immunosorbent assay; EPR, electron paramagnetic resonance; ER-β, estrogen receptor β; GSH, glutathione; GOX, glucose oxidase; HIV, human immunodeficiency virus; FRET, fluorescence resonance energy transfer; FWHM, full-width-at-half-maximum; PB, Pacific Blue; PCR, polymerase chain reaction; PDDA, poly(diallyldimethylammonium chloride); PEG, polyethylene glycol; PET, photoinduced electron transfer; PIGE, paraffin impregnated graphite electrode; PL, photoluminescence; L-Cys, L-cysteine; LOD, limit of detection; MAA, mercaptoacetic acid; MBP, maltose binding protein; MB, molecular beacon; MPA, mercaptopropionic acid; MMP, matrix metalloproteinase; MSP, methylation specific polymerase chain reaction; NAD, nicotinamide adenine dinucleotide; ${}_{x}QD_{w}$, quantum dot (peak PL at *w* nm, first exciton peak at *x* nm); RhR, Rhodamine Red; Rluc, *Renilla* luciferase; RRE, rev responsive element; SA, Streptavidin; SCE, standard calomel electrode; SMD, single molecule detection; SNP, single nucleotide polymorphism; TAMRA, carboxytetramethylrhodamine; TBA, thrombin binding aptamer; VB, valence band.

* Corresponding author. Tel.: +1 905 828 5437; fax: +1 905 569 4388.
E-mail address: ulrich.krull@utoronto.ca (U.J. Krull).

0003-2670/$ – see front matter © 2010 Elsevier B.V. All rights reserved.
doi:10.1016/j.aca.2010.05.026

1. Introduction

Quantum dots (QDs) are one of several types of nanomaterial that have had a significant impact on research in many fields across the physical, chemical, and biological sciences. QDs are semiconductor nanocrystals that generally have dimensions in the range of 2–6 nm. Multidisciplinary interest in QDs has been largely motivated by their unique electro-optical properties that lie between the molecular and bulk semiconductor regimes [1]. Although QD research gained momentum in the early 1990s, it was arguably the adoption of QD-bioconjugates as fluorescent labels for biological imaging [2,3] that catalyzed significant interest across the bioanalytical, biophysical, and biomedical research communities at the turn of the century. QDs are recognized as frequently providing better brightness and photostability compared to conventional fluorescent dyes, while also being better suited for multicolour applications [4]. At present, QDs continue to make an impact in these fields through cellular, tissue, or whole body imaging [4–8], and the development of optical probes for biological sensing [4,5,9–12].

This review addresses the development of bioassays, bioprobes, and biosensors utilizing QDs as an integrated component of the analysis. We make a distinction between "non-integrated" and "integrated" QDs based on design. A non-integrated QD is one that is selectively introduced to a bioanalysis as a consequence of biorecognition. Examples include the use of QDs as fluorescent labels in microarrays [13,14], or electroactive labels in assays based on anodic stripping voltammetry [15]. In contrast, an integrated QD is one that is present in a system throughout a bioanalysis—it simultaneously has a role in transduction and as a scaffold for biorecognition. In many cases, this requires the direct conjugation of affinity probes or biorecognition elements to a QD, or their co-assembly at an interface. The key point is that transduction occurs by modulating QD luminescence between high/low or on/off states. The bioassays, bioprobes, and biosensors discussed herein are primarily limited to those with integrated QDs and optical transduction.

The modulation of QD luminescence as a selective response to the presence of target analyte can be achieved in several ways. These include, but are not necessarily limited to: fluorescence resonance energy transfer (FRET), bioluminescence resonance energy transfer (BRET), charge transfer (CT) quenching, and electrochemiluminescence (ECL). The photoluminescence (PL) of QDs is strongly influenced by CT reactions, while QDs have been demonstrated to be excellent donors in FRET and acceptors in BRET. The strong distance dependence of these processes has provided the basis for many detection strategies. Biorecognition events are used to modulate distances between proximal redox active species, chromophores, or fluorophores. Concomitant changes in PL spectra and intensity provide an analytical signal. The modulation of ECL intensity from QDs using analyte reactivity, enzyme turnover, or changes in co-reactant mass transport has also been used to provide an analytical signal. The basic principles underlying these detection strategies are presented in this review, along with an overview of their applications in the selective detection of small molecules, ions, nucleic acids, proteins, enzymes, and other biologically important targets. Some special attention is given to recent developments in solid-phase assays, which can provide unique advantages compared to their more widely employed solution-phase counterparts. The review of analytical applications is prefaced by a brief overview of QDs, with emphasis on their interfacial chemistry and bioconjugation.

2. Quantum dots: surface chemistry and conjugates

2.1. Quantum dots

The unique electro-optical properties of QDs arise from the combination of material and dimensionality, the latter known as "quantum confinement" [4,5,16,17]. Despite the emergence of other materials [18–25], the most popular material choices remain CdSe and CdTe [1,26–34]. The synthetic methods and characterization for high-quality QDs composed of these materials are widely available, and PL in the visible and near-IR regions of the spectrum is obtained. Typically, core–shell structures with an inorganic capping layer of ZnS around the core nanocrystal are used to improve luminescence properties (e.g. CdSe/ZnS) [26,29,30,34]. The favorable optical properties of QDs include: strong, broad, one-photon and two-photon absorption; narrow, symmetric, size-tunable PL (full-width-at-half maximum, FWHM, ca. 25–35 nm); potentially high quantum yield (>20%); and generally long PL decay times (often > 10 ns) [4,5,17,35]. Other, often less desirable, optical features of QDs can include: multi-exponential PL decay, bluing, brightening, and blinking at the single QD level [36].

Due to the large surface area-to-volume ratios of QDs, the quality and characteristics of the nanocrystal surface are tantamount to the quality of the core in determining the observed PL properties. Decreases in quantum yield, changes in PL decay, spectral shifts, and the appearance of undesirable band-gap PL can be associated with surface states. The growth of a high-quality inorganic shell around the core nanocrystal reduces the impact of surface states on PL. However, the influence of the QD surface cannot be eliminated; adsorbates, ligands, or other coatings can affect PL properties. This is not necessarily a detriment—the ability of core carriers (i.e. electrons and holes) to interact with states in the surrounding matrix are essential in many applications involving CT. Surface chemistry is a critically important consideration in developing all types of assays, bioprobes, and biosensors based on QDs. In addition to retaining the favourable optical properties of QDs,

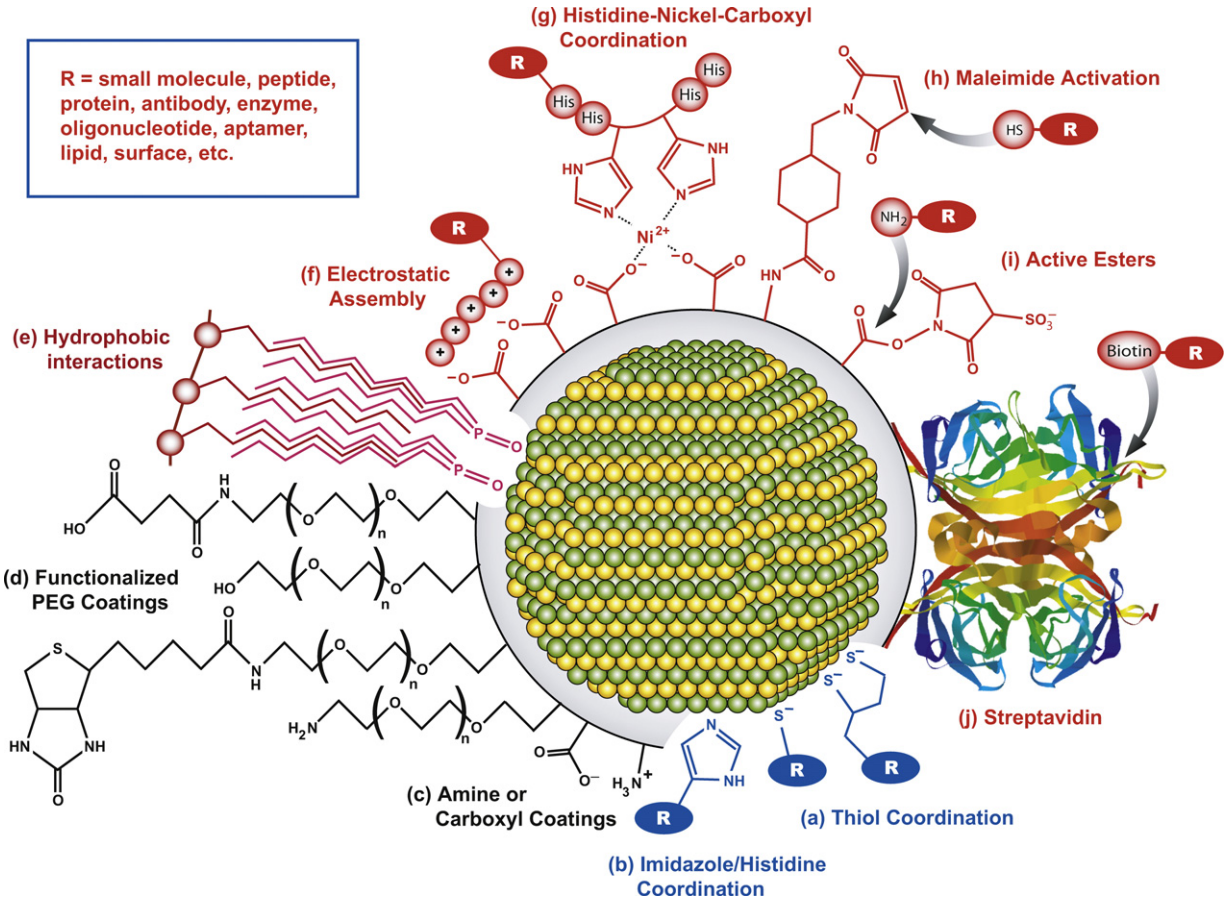

Fig. 1. An illustration of some selected surface chemistries and conjugation strategies that are applied to QDs. The grey periphery around the QD represents a general coating. This coating can be associated with the surface of the QD via (e) hydrophobic interactions, or ligand coordination. Examples of the latter include: (a) monodentate or bidentate thiols, (b) imidazole, polyimidazole (e.g. polyhistidine), or dithiocarbamate (not shown) groups. The exterior of the coating mediates aqueous solubility by the display of (c) amine or carboxyl groups, or (d) functionalized PEG. Common strategies for bioconjugation include: (a) thiol modifications or (b) polyhistidine or metallothionein (not shown) tags that penetrate the coating and interact with the surface of the QD; (f) electrostatic association with the coating; (g) nickel mediated assembly of polyhistidine to carboxyl coatings; (h) maleimide activation and coupling; (i) active ester formation and coupling; (j) biotin-labeling and streptavidin–QD conjugates. Figure not to scale.

the surface chemistry of choice should also allow bioconjugation, impart aqueous solubility, and not impede the efficient use of FRET, BRET, CT, or ECL as a transduction method. With respect to efficient transduction, the thickness of the coating is a very important consideration. Many of the studies described in this review have used compact ligand-based QD coatings to minimize thickness, although polymer and polymer–protein coated QDs have also been successfully used in FRET and BRET methods.

QDs are coated with organic molecules and macromolecules to provide aqueous solubility and opportunities for bioconjugation. These coatings can be broadly classified as ligand-based or polymer-based, and neutral or charged. Some of these general strategies are illustrated in Fig. 1. Ligand coatings are comprised of small molecules that coordinate directly to the inorganic surface of the QD. The most common ligands have been monodentate (e.g. mercaptopropionic acid, MPA) or bidentate (e.g. dihydrolipoic acid, DHLA) thiols with terminal carboxylate groups [4,35]. These ligands are compact, charged, and colloidal stability is maintained via electrostatic repulsion. Aggregation often results in low pH or high ionic strength solutions [37–39]—the latter being particularly common in biological matrices, and the former being characteristic of cellular lysosomes. Zwitterionic thiol terminated ligands such as penicillamine [40] or cysteine [41] can improve stability over a range of pH values. In addition, a diverse array of polyethylene glycol (PEG) appended ligands has been used to coat QDs [42–46]. These ligands do not depend on charge for solubility, and offer superior colloidal stability across a large range of pH and ionic strengths, low non-specific binding, and biocompatibility. Similar to thiols, dithiocarbamate ligands have also been found to coordinate to the QD surface, but their use has been more limited [47,48].

Polymeric coatings have traditionally been based on amphiphilic polymers, where assembly on the QD is driven by the hydrophobic interactions of pendant alkyl chains with the native ligands (e.g. TOPO from synthesis) of the QD [49,50]. However, a polymer coating has recently been developed with pendant imidazole groups that coordinate directly to the QD surface and displace (at least partially) the native ligands [51]. At the expense of larger hydrodynamic size and coating thickness, polymer coatings often give brighter QDs than ligand coatings [52,53]. Carboxyl groups, amine groups, PEG groups, or combinations thereof are generally used as the hydrophilic component of amphiphilic polymers. Polymer coated QDs are available commercially with amine groups, carboxyl groups, or Streptavidin (SA) modifications. The latter is particularly popular due to the ease of bioconjugation.

2.2. Bioconjugation

The preparation of QD-bioconjugates is essential to the development of assays, bioprobes, and biosensors. Fig. 1 illustrates several common strategies. Enzymes [54,55], antibodies [56–58], small molecule binding proteins [59–61], and oligonucleotides [62–66] are among the biorecognition agents that can be coupled to QDs. For example, the reduction of the disulfide bridges of antibodies provides a convenient route to available thiol groups [57,67].

These, as well as cysteine residues in other proteins (often introduced by site-directed mutagenesis), can be coupled to maleimide activated QDs [58,68]. The lysine residues of proteins can also be coupled with carbodiimide or succinimide ester activated QDs [69]. Synthetic oligonucleotides with thiol or amine modifications are widely available and can be analogously conjugated to QDs [62,64]. Although successful in many applications, conjugation via cross-linking has several potential drawbacks. Protein orientation at the QD surface is often not controlled, and undesirable protein–protein cross-linking or protein mediated QD–QD cross-linking can also occur. Furthermore, competing hydrolysis reactions and the need for excess cross-linker can result in poor control over conjugate valence (i.e. the number of biomolecules per QD). In addition, if the activation of charge stabilized QDs with a charge-neutralizing cross-linker is excessive, aggregation may occur due to the loss of stabilizing functional groups. Furthermore, certain buffer compositions and pH values are not compatible with some coupling agents, or may reduce the efficiency of others. For example, carbodiimide coupling is poorly compatible with amine or phosphate containing buffers, and optimal reactivity is achieved at pH < 6 [70] where the colloidal stability of carboxyl coated QDs is not optimal.

An alternative to cross-linking strategies is the self-assembly of QD-bioconjugates. For example, proteins appended with polyhistidine [71–74] or metallothionein [75] tags spontaneously coordinate to the inorganic surface of QDs, and provide stable conjugation with nanomolar dissociation constants. This approach provides much better control over protein orientation [76], avoids undesirable protein–protein or QD–QD cross-linking, and has fewer buffer restrictions. The polyhistidine method has also been extended to the preparation of QD–oligonucleotide conjugates [77,78]. Similarly, thiol terminated oligonucleotides can be used for the self-assembly of QD–oligonucleotide conjugates [63,79]. Ligand coated QDs are best suited for these methods as they allow access to the inorganic surface of the QD and have some lability.

Denticity is an important consideration in experiments that use ligand coatings and the self-assembly of bioconjugates. While polyhistidine tags have been shown to assemble on DHLA coated QDs, the displacement of bidentate thiol ligands by monodentate thiol modified oligonucleotides is not favoured. However, the latter is compatible with monodentate thiol (e.g. MPA) ligand coated QDs. Moreover, the polyhistidine tags are also compatible with carboxy-polymer coatings. Although the QD surface is not accessible, nickel (II) ions can serve as bridge through mutual chelation by the carboxylate groups and histidine moieties [80]. Electrostatic self-assembly is also compatible with both ligand and polymer coatings. Through the control of pH, either the native p*I* of a protein, or charge associated with an engineered tag [59,81], can drive association with an oppositely charged QD. Cationic polymers have also been used to mediate the assembly of oligonucleotides around negatively charged QDs. However, electrostatic strategies are limited by their pH dependence and the potential for dissociation at high ionic strength. Overall, perhaps the biggest advantage of self-assembly methods is the greater level of control over conjugate valence. The QDs and biomolecules can be mixed in stoichiometric quantities to obtain the desired conjugate valence, albeit an average subject to a Poisson distribution [82].

The well-known biotin–SA binding interaction is perhaps the most widely used method for the preparation of QD-bioconjugates. This has included: antibodies [81], peptides [83], proteins [84], oligonucleotides [65], and aptamers [66]. Assuming a relatively narrow distribution of available binding sites across a population of QD–SA conjugates, this method also provides good control over conjugate valence. If biotinylation is site-specific [85], there is also a degree of control over bioconjugate orientation. The commercial availability of both QD–SA conjugates, and biotinylated biomolecules (or biotinylation kits), contributes to the popularity of this method. Conversely, biotinylated ligands have been developed for QDs and potentiate conjugation using Avidin bridges [86] or with Avidin fusion proteins.

Other conjugation strategies, such as ligation methods [87,88], continue to be developed with QDs. The novelty is not necessarily in the chemistry, but in the application to nanoparticles. Researchers in the field have realized that the chemical and biochemical toolboxes have not been tapped to their full potential. In particular, the development of simple and efficient coupling chemistry that is orthogonal to common biological functions (e.g. $-NH_2$, –COOH, –SH) will be highly advantageous for the preparation of QD-conjugates with synthetic oligonucleotides or peptides. Such chemistries would also facilitate the preparation of mixed conjugates for the controlled display of more than one unique biomolecule. That is, for example, two different peptide or oligonucleotide sequences, or a peptide and an oligonucleotide in combination. Continued advances in QD coatings and bioconjugation will enable continued advances in the development of QD-based bioanalyses.

3. Transduction mechanisms

3.1. Fluorescence resonance energy transfer

The theory and applications of FRET have been thoroughly reviewed elsewhere [89], and are generally well known. This section emphasizes aspects of FRET that are unique or important to QDs. Selected applications of QDs and FRET in biological sensing are also presented, and additional examples can be found in previous reviews on the subject [10,12,90]. The basis of the majority of assay and bioprobe development is the distance dependence of FRET. In general, QDs serve as energy donors, and biomolecules are labeled with an acceptor dye. Biorecognition events at the surface of the QDs are used to drive the association or dissociation of acceptors, or alter the QD-acceptor separation distance. The resulting modulation of FRET efficiency provides an analytical signal.

3.1.1. FRET and QDs

QDs are excellent donors in FRET and have several unique advantages when compared to molecular fluorophore donors. It is instructive to consider these advantages in the context of two key results of the Förster formalism: the efficiency–distance relationship (Eq. (1)), and the Förster distance (Eq. (2)). It will be seen that QD donors offer several potential advantages in FRET. In Eq. (1), E is the energy transfer efficiency, R_0 is the Förster distance, r_i is the distance between the donor and the ith acceptor, and a is the total number of acceptors. The Förster distance is characteristic of a donor–acceptor pair and is the distance at which the FRET efficiency is 50%. In Eq. (2), κ^2 is the orientation factor, Φ_D is the quantum yield of the donor, J is the spectral overlap integral, n is the refractive index of the medium, N is Avogadro's number, $F_D(\lambda)$ is the donor fluorescence, $\varepsilon(\lambda)$ is the acceptor molar absorption coefficient, and λ represents wavelength.

$$E = \frac{\sum_i^a (R_\circ/r_i)^6}{1+\sum_i^a (R_\circ/r_i)^6} \approx \frac{aR_\circ^6}{r^6 + aR_\circ^6} \quad (1)$$

$$R_\circ^6 = \frac{9(\ln 10)\kappa^2 \Phi_D J}{128\pi^5 n^4 N} = 8.79\times10^{-28}\ \text{mol}^{-1}\cdot\kappa^2\Phi_D n^{-4}\frac{\int F_D(\lambda)\varepsilon_A(\lambda)\lambda^4 d\lambda}{\int F_D(\lambda)d\lambda} \quad (2)$$

First, consider the efficiency–distance relationship in Eq. (1). QDs provide the opportunity for the interaction of a single donor (i.e. the QD) with multiple acceptors via assembly at the QD surface (e.g. labeled biomolecules). In such systems, there is often the potential for each individual acceptor to be located at a slightly different distance from the donor, or to sample slightly different

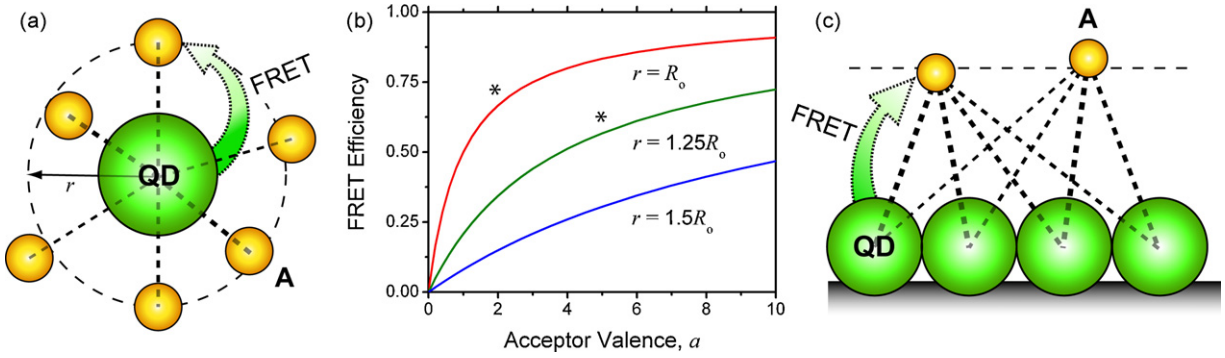

Fig. 2. Different FRET-configurations: (a) an approximately centrosymmetric arrangement of acceptors around a single colloidal QD donor; (b) FRET-efficiency at different donor–acceptor separations, r, as a function of conjugate valence, a, where R_0 is the Förster distance; (c) multiple donor–acceptor interactions over a distribution of distances using an immobilized film of QDs.

orientations. However, these differences are usually neglected, and spherical symmetry is assumed, as shown in Fig. 2a. This yields the final result in Eq. (1), where each acceptor is considered to be equivalent. A key advantage of using multiple acceptors is being able to drive more efficient FRET. Moreover, control of acceptor valency around the QD provides the opportunity to tune FRET efficiency without changing the donor–acceptor pair or separation distance. For example, as shown in Fig. 2b, the assembly of 1, 2, 3, or 6 acceptors around a QD at the Förster distance results in FRET efficiencies of 50%, 67%, 75%, and 86%, respectively.

Next, consider Eq. (2), where a high donor quantum yield and a large donor–acceptor spectral overlap integral are important in maximizing the Förster distance. For example, 2-, 4-, or 10-fold changes in either quantity result in 12%, 26%, and 47% increases in the Förster distance. Since the quantum yield of QDs is generally high, a large Förster distance is favoured. Furthermore, the size-tunable PL of QDs provides an opportunity for maximizing the Förster distance by tuning the spectral overlap integral continuously over a range of values (cf. discrete steps with different molecular fluorophores). In addition, the narrow PL spectrum of QDs allows the spectral overlap to be maximized without necessitating a large degree of overlap between the emission spectra of the donor and a fluorescent acceptor (cf. the red tail of molecular donor fluorophores), allowing better resolution of the two signals.

Another advantage is afforded by the broad absorption spectrum of QDs. In the ideal FRET experiment, none of the acceptor dye molecules are directly excited by the light source. However, in practice, a small, but increasing percentage of acceptors are directly excited as the excitation wavelength approaches their first or second excited state transitions. Since only a ground-state acceptor dye can participate in FRET, this implies that the effective value of a in Eq. (1) can be less than the nominal value of a. The direct excitation of acceptors can be minimized with QD donors because donor excitation is efficient over a wide wavelength range, making it easier to work far from wavelengths associated with acceptor dye transitions. The high molar absorption coefficients and potentially high quantum yields of QDs also allow the use of lower intensity excitation, further minimizing the direct excitation of acceptors, and also minimizing photobleaching rates.

The above discussion has tacitly assumed that the Förster formalism – derived for two point-dipoles – is applicable to QDs. On the basis of theoretical calculations, Allan and Delerue [91], and Curutchet et al. [92] determined that the Förster formalism is applicable to direct band-gap semiconductor nanocrystals. An interesting result of the latter study is that the dipole–dipole approximation remains a good model even at contact distances between a QD and an acceptor. This is in contrast to molecular dyes, where the point dipole approximation fails at separation distances similar to the molecular dimensions. Similarly, it was not clear that the Förster formalism was valid given the large size of QDs compared to dye molecules, and a size that is comparable to the typical 2–6 nm donor–acceptor separations in FRET experiments. However, the CdSe QD transition density effectively behaves as a positive charge and negative charge localized at the center of the nanocrystal and separated by a 0.7 nm distance—i.e. a dipole [92]. Therefore, despite the volume of a QD occupying a sphere several nanometers in diameter, donor–acceptor distances should be calculated from its center. Thus, the radius of the QD imposes a minimum center-to-center separation with an acceptor, ensuring the applicability of the Förster formalism for dye acceptors positioned outward from the QD surface. Of course, this does not preclude the possibility of other short-range energy transfer processes (e.g. CT) competing with FRET.

The outcomes of a multitude of experimental studies are in agreement with the expectations derived from theoretical analyses. FRET efficiencies have been found to scale with the value of the spectral overlap integral, the number of proximal acceptors, and the minimum donor–acceptor separation imposed by the QD (for example [93]). Moreover, FRET efficiencies measured from both steady-state and time-resolved PL measurements have shown generally good agreement with predictions derived from geometric estimates and the inverse sixth dependence (r^{-6}) of the Förster formalism (Eqs. (1) and (2)). For example, using a rigid polypeptide as a variable length spacer, Pons et al. [94] and Medintz et al. [95] have observed excellent agreement between measured and predicted FRET efficiencies as a function of changes in the QD donor–acceptor dye separation. Good correspondence between ensemble and single-pair FRET-derived distance measurements [82] further suggests the applicability of the Förster formalism. However, the inhomogeneous broadening of the QD PL spectrum (i.e. nanocrystal size distribution) does introduce a feature somewhat unique to QDs. Individual QDs associated with the hypsochromic and bathochromic edges of the overall PL spectrum can have different energy transfer rates as a function of the slope of the acceptor absorption spectrum. This can appear in the ensemble spectrum as an apparent shift in the position of the peak PL [96]. Reformulations of the spectral overlap integral have been developed to address inhomogeneous broadening [97], but the calculation of J in Eq. (2) should nonetheless be a good first approximation in many cases, and narrower size-distributions will minimize the error.

In the vast majority of experimental studies, the value of the orientation factor is assumed to be $\kappa^2 = 2/3$. In order for this assumption to be strictly valid, the donor and acceptor transition dipoles must sample an isotropic distribution during the donor excited state lifetime (i.e. rapid rotation and a random orientation

Table 1
Summary of the use of QDs as integrated components of bioassays, bioprobes, or biosensors by application and reference number.

Biorecognition	Transduction			
	FRET	BRET	CT Quench.	ECL
DNA/RNA hybridization	64, 65, 77, 119–123, 125–131, 208–211, 234–237	149	–	205
Aptamer–protein/peptide complex	66, 108, 112–114, 118	–	177	–
Aptamer-small molecule complex	109, 110, 115, 116	–	–	–
Protein-small molecule binding	60, 95, 238	–	163, 174–176, 178	–
Immunocomplex	56, 57, 144, 145, 231	–	–	201–204
Protease or nuclease activity	79, 136–143	80, 87	161, 179, 180	–
Enzyme–substrate reaction	–	–	180, 239	197, 200, 207
Small molecule/ion complexes/reactivity	104–106	–	158, 159, 164, 181	193, 196, 198, 206, 207
Macromolecular complexes	132–135	–	–	–

relative to one another). However, CdSe QDs have been shown to have a dark axis (their *c*-axis), with a doubly degenerate transition dipole (i.e. circular emitter) in the orthogonal plane [98]. Therefore, the assumption that $\kappa^2 = 2/3$ is not strictly valid, and different values of κ^2 may apply to proximal acceptors at different positions relative to the *c*-axis. Nonetheless, the error introduced by the assumption appears to be small in most experiments. The partially random orientation of the QD transition dipole, combined with the (usually) random and dynamic orientation of the acceptor transition dipole, as well as the distribution of proximal acceptor positions across an ensemble, allow $\kappa^2 = 2/3$ to be a useful first approximation.

While QDs offer numerous advantages as donors in FRET, there are some caveats. The radius of a QD adds a fixed amount to the donor–acceptor separation. Therefore, as much as the QD size can tune the spectral overlap integral and FRET efficiency, there is also an inherent minimum donor–acceptor distance due to the QD radius. The need to derivatize QDs with coatings can add additional distance. Unfortunately, thicker coatings, which are unfavourable for FRET, are usually associated with higher QD quantum yields, which are favourable for FRET, and vice versa. In general, the best compromise needs to be determined for each individual system. Finally, despite their advantages as donors, QDs are poor acceptors when combined with molecular dyes as donors in FRET [99]. While their broad absorption can result in very large spectral overlap integrals, it also results in very efficient and unavoidable direct excitation, regardless of excitation wavelength. This is compounded by the typical lifetime mismatch between QDs (often >10 ns) and dye donors (usually <10 ns). As a consequence, the QDs are rarely in the ground state while a dye is in an excited state, and thus the number of available QD acceptors is negligible. However, the use of QDs as acceptors has been demonstrated using other QDs as donors [100], and by using lanthanide donors [101,102]. In these systems, the donor lifetime is comparable to, or longer than, the QD acceptor lifetime. In the case of long-lifetime (∼ms) lanthanide donors, time-gating has been used to separate the FRET-sensitized QD PL from the comparatively short-lived PL from direct excitation. This approach has been used to develop immunoassays [101,102]. We speculate that lanthanide donors with efficient fluorescence upconversion could overcome the requirement of time-gating, and permit steady state measurements with minimal direct excitation of QDs. As described in Section 3.2, QDs are also good acceptors in BRET experiments, where donors are not excited optically.

3.1.2. Applications

Bioassays and bioprobes that use QDs as donors in FRET are the most developed and widespread approach to integrating QDs into bioanalyses. This section summarizes selected examples of small molecule detection, the use of aptamers as affinity probes, hybridization assays, nuclease and protease detection, and immunoassays. A categorized list of the cited references is given in Table 1. Examples of sensing schemes are illustrated in Fig. 3, and general transduction formats are illustrated in Fig. 4. The notation QD_w is used to indicate a peak QD PL position at *w* nm. Moreover, the reader should assume that the QD material is CdSe/ZnS unless otherwise noted.

A review of biological sensing using QDs and FRET is not complete without noting the early contributions to the field that were made by the research teams of Medintz and Mattoussi. One focus of their research was the use of dye labeled protein–QD conjugates to elucidate the fundamental spectroscopic properties of QDs as donors or acceptors in FRET. Many of these studies were cited in the Section 3.1.1. Another important focus of their research was the development of QDs as donors in FRET for biological sensing. Self-assembled QD–maltose binding protein (MBP) conjugates, where maltose was the target analyte, provided the basis for the development of several FRET-based transduction strategies. The interested reader is referred to many other reviews for summaries of these important contributions [10,12,103], and some of the original references are cited in Table 1.

A glucose bioprobe was developed by Tang et al. using CdTe QD_{530} modified with concanavalin A (ConA), and gold nanoparticles (Au NPs) modified with β-cyclodextrin (β-CD) [61]. In the absence of glucose, the ConA bound the β-CD and created proximity between the QDs and the Au NPs that caused fluorescence quenching. The addition of glucose resulted in a competition for the ConA binding sites where some of the β-CD was displaced. The loss of the proximity between the QD and Au NP restored the QD PL intensity to a degree that was proportional to the glucose concentration. The limit of detection (LOD) for the method was 50 nM, and the bioprobe retained its function in human serum. The competitive binding strategy was analogous to that used in the seminal work by Medintz et al. for the detection of maltose using QD–MBP conjugates and FRET [60].

Freeman and coworkers developed a method for the detection of monosaccharides or dopamine using QDs coated with boronic acid ligands [104]. These ligands form complexes with glucose, galactose, and dopamine. A competitive binding assay was developed using galactose or dopamine labeled with Atto-590 dye. Unlabeled target analyte in the sample competed for binding sites with the labeled analyte. The ratio of QD_{570}-to-Atto-590 emission provided the analytical signal and decreased with increasing glucose, galactose, or dopamine in the sample. The corresponding LODs were 1, 50, and 100 μM, respectively. However, the selectivity of these assays was poor due to the potential response to any *cis* diol in a sample. The same research group also developed a QD-FRET probe to study intracellular metabolism [105]. CdSe/CdS/ZnS multi-shell QD_{635} were functionalized with Nile Blue dye as a dark quencher. A protein layer between the dye and QD was necessary to block CT quenching in preference to FRET. The transduction of metabolism (Fig. 3a) relied on the reduction of Nile Blue by reduced nicotinamide adenine dinucleotide (NADH). As a consequence of its reduction, the absorbance of Nile Blue shifted, and the spectral overlap with the QD donor vanished, preventing efficient FRET and restoring QD PL (Fig. 4a,ii). To demonstrate the ability to monitor

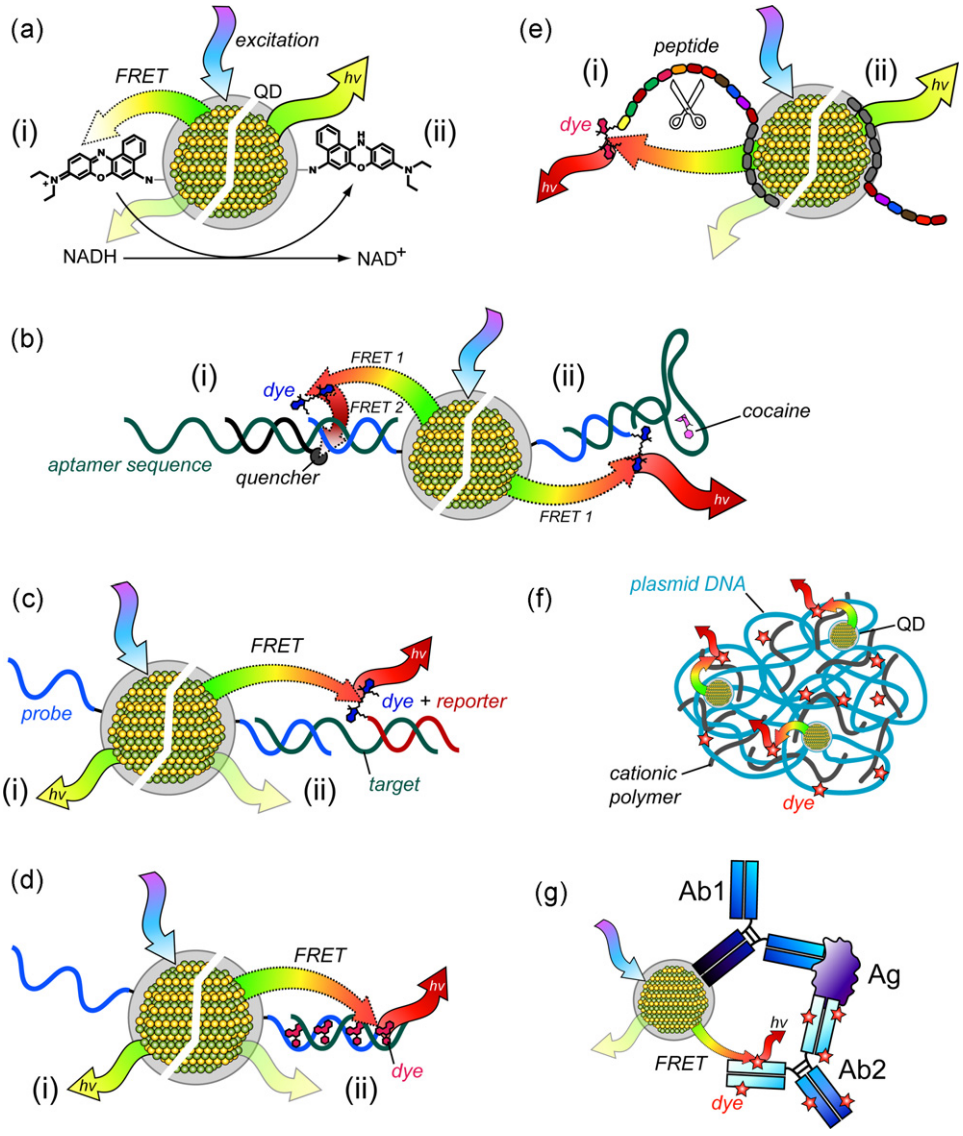

Fig. 3. (a) A FRET-based assay for probing the activity of enzymes that depend on the NAD^+ cofactor. In (i) the Nile Blue dye has spectral overlap with the QD and FRET occurs. In (ii) the reduced form of Nile Blue (NADH as the reducing agent) does not have spectral overlap with the QD, and FRET is quenched, restoring the QD PL [105]. (b) A tripartite aptamer-based probe for the detection of cocaine [110]. In (i) two-step FRET occurs from the QD to a fluorescent acceptor dye, and then to a dark quencher. These are labels on oligonucleotides hybridized to the aptamer sequence. (ii) When the aptamer binds cocaine, the dark quencher-labeled oligonucleotide is displaced, restoring single step FRET. The FRET-sensitized acceptor dye PL is restored. (c) A sandwich format for a nucleic acid hybridization assay [65]. The hybridization of unlabeled target with (i) a probe oligonucleotide and (ii) an acceptor dye-labeled reporter oligonucleotide provides the proximity for FRET, quenching the QD PL. (d) A nucleic acid hybridization assay using an intercalating dye as an acceptor [123,125]. The hybridization of unlabeled target with (i) a probe oligonucleotide creates (ii) double-stranded DNA, with which the intercalating dye binds. This provides the proximity for FRET and quenches the QD PL. (e) A protease assay where (i) an acceptor dye-labeled peptide is assembled on a QD donor via a polyhistidine tag [138]. The QD-dye proximity in the bioconjugate is sufficient for FRET. (ii) Protease activity (scissors) cleaves the peptide and quenches FRET, restoring the QD PL. (f) Polyplex assembly incorporating dye-labeled cationic polymer, and QD-labeled plasmid DNA. The proximity in the polyplex is sufficient for FRET. Unpacking of the DNA removes this proximity, and quenches FRET (not shown) [132–135]. (g) A sandwich immunoassay using a QD labeled monoclonal antibody and acceptor dye-labeled polyclonal antibody. The donor–acceptor proximity in the immunocomplex is sufficient for FRET [57]. Figures not to scale.

the activity of any NAD^+/NADH dependent enzymes, the activity of alcohol dehydrogenase was measured *in vitro*. The QD-Nile Blue conjugates were then introduced to cancer cells by electroporation, and used to monitor changes in metabolism upon the introduction of D-glucose and taxol. An increase in QD PL signaled an increased metabolism in the case of the former; a decrease in QD PL signaled a decreased metabolism in the case of the latter. Snee et al. have also used the concept of switching the acceptor dye absorption in and out of resonance with the QD emission for pH sensing [106].

The use of aptamers in analyses has continued to grow, and this includes reports of QD-aptamer conjugates as bioprobes. The in vitro selection, chemical synthesis, high binding affinities, robustness, and conformation-switching properties of aptamers are very attractive for the development of bioprobes and biosensors. Levy et al. developed the first QD-aptamer bioprobe for FRET-based sensing of thrombin [66]. Transduction was based on the structure-switching signaling mechanism introduced by Nutiu and Li [107], where a Watson–Crick base-paired oligonucleotide is displaced from the aptamer in preference to secondary-structure driven target binding. Levy et al. demonstrated that a short dark quencher-labeled complementary oligonucleotide could be displaced from a QD_{525}-thrombin binding aptamer (TBA) conjugate upon the introduction of thrombin, restoring QD PL and providing an analytical signal [66]. This strategy has been adopted by a number of other research groups using different aptamers. For example, Kim et al. used a dark quencher with QD_{600}–aptamer conjugates for the

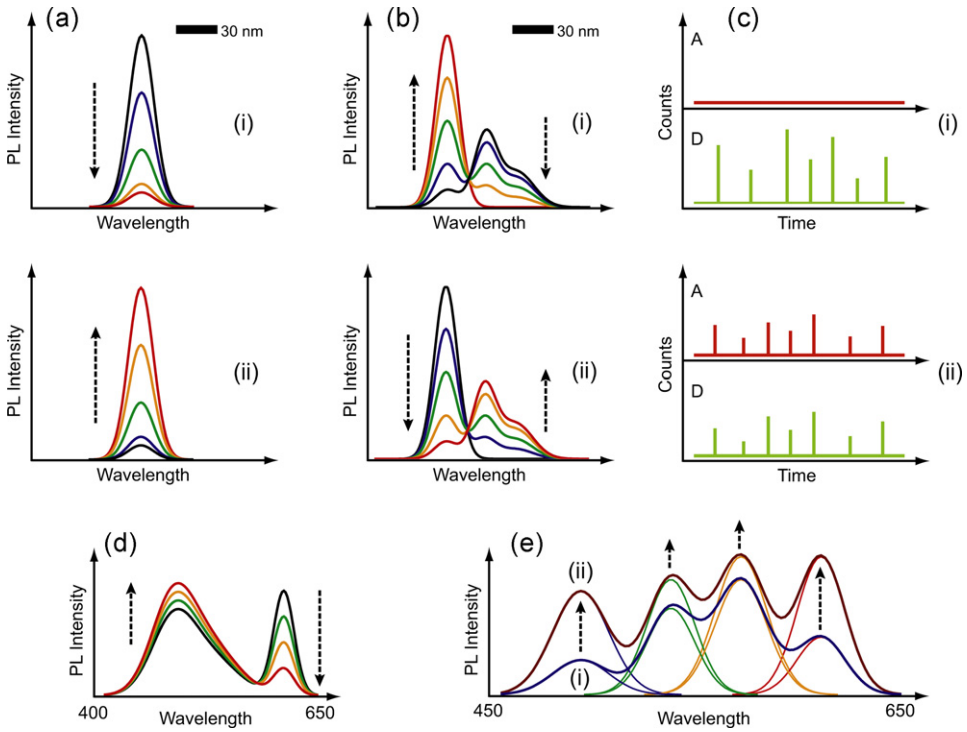

Fig. 4. Basic forms of experimental data associated with the transduction of biorecognition events using QDs and resonance energy transfer. (a) FRET-based transduction at the ensemble level using a QD donor and a dark quencher as an acceptor: (i) PL quenching or (ii) PL recovery with increasing amounts of target analyte. (b) FRET-based transduction at the ensemble level using a QD donor and a fluorescent acceptor: (i) the loss of FRET-sensitized acceptor PL or (ii) the evolution of FRET-sensitized acceptor PL with increasing amounts of target analyte. (c) FRET-based transduction using a QD donor and fluorescent acceptor at the single molecule level via burst analysis: (i) no FRET interaction or (ii) FRET interaction. (d) BRET-based transduction using a QD acceptor with a coelenteramide donor (from luciferase activity). A decrease in BRET with an increasing amount of target analyte is shown. (e) A multiplexed configuration of QD donors and dark quenchers as acceptors. Different extents of PL recovery are shown for each QD donor between (i) and (ii). The reader is referred to reference [240] for a demonstration of multiplexed FRET quenching. In parts (a)–(e), the dashed arrow indicates the trend with increasing amounts of target analyte.

detection of platelet derived growth factor [108]. The dynamic range of this bioprobe was from 0.4 to 1.6 nM. Similarly, Chen et al. used a QD_{605}-Cy5 FRET-pair with an adenosine triphosphate (ATP) binding aptamer [109]. The decrease in the ratio of FRET-sensitized Cy5 PL-to-QD PL provided an analytical signal with linear response from 0.1 to 1.0 mM and a LOD of 24 μM. Similarly, Zhang and Johnson used a Cy5-labeled oligonucleotide as an acceptor for QD_{605}-cocaine binding aptamer conjugates [110]. The loss of FRET-sensitized Cy5 PL was proportional to the concentration of cocaine down to a LOD of 0.5 μM. However, rather than working with only a "Cy5-off" configuration for generating analytical signal, these researchers also demonstrated a "Cy5-on" configuration (Fig. 3b) by assembling a tripartite FRET-system with a QD donor, and both Cy5 and a dark quencher acceptors. The latter quenched both the QD and Cy5 PL via FRET, where both direct quenching of the QD, and relay quenching of the FRET-sensitized Cy5 excitation were possible (albeit with different probabilities). Cocaine binding displaced the dark quencher, restoring FRET-sensitized Cy5 PL as the analytical signal.

The above study by Zhang and Johnson was also significant because of the instrumentation associated with the method: single molecule detection (SMD) and the use of capillary flow. In contrast to ensemble measurements, both low- and high-efficiency FRET can be readily resolved in single-pair FRET experiments via SMD and burst count analysis (Fig. 4c). In addition, these authors found that the FRET efficiency was enhanced by the deformation of nucleic acids in a flowing solution inside a microcapillary column [111]. Thus, the combination of capillary flow and single molecule spectroscopy provides the opportunity for more sensitive detection. This can relax some of the geometric constraints in the design of QD-conjugates for FRET-base bioprobes, and improve LODs. Zhang and Johnson have also developed a model assay for measuring the interaction between the human immunodeficiency virus (HIV) regulatory protein, Rev, and the Rev responsive element (RRE) within the *env* gene of the HIV-1 RNA genome [112,113]. The *in vitro* model consisted of a Cy5-labeled peptide sequence derived from the Rev protein, and a biotinylated stem-loop IIB ribonucleotide sequence of RRE assembled on a Streptavidin-coated QD_{605}. These peptide and ribonucleotide sequences are responsible for the secondary structure driven binding interaction between the native biomolecules. FRET-sensitized Cy5 PL provided an analytical signal proportional to Rev-peptide binding, and enabled the measurement of dissociation constants—including the inhibition of Rev-RRE binding by proflavin or neomycin B. Measurement via single-pair FRET allowed the resolution of the QD-Cy5 FRET process against a large background of proflavin fluorescence, without the spectral deconvolution that would have been necessary in ensemble measurements.

The dissociation of acceptor-labeled duplex nucleic acid upon aptamer binding events is not the only strategy for FRET-based transduction. Researchers have developed a number of other aptamer-based strategies for switching FRET between "on" and "off" states through association or dissociation, and without the labeling of small molecule or protein targets. For example, Cheng et al. [114] developed an aptameric QD-FRET probe for the detection of mucin 1—an epithelial cell surface glycoprotein that is a biomarker useful in early diagnosis of several cancers. The probe design consisted of a QD_{530}-labeled reporter oligonucleotide, a dark quencher labeled oligonucleotide, and a third oligonucleotide sequence incorporating an aptameric region that binds mucin 1. Transduction was based on a change in secondary structure of the mucin 1 aptamer upon binding. This allowed the QD-

labeled reporter oligonucleotide to hybridize to a portion of the aptamer sequence adjacent to a region that had hybridized with quencher-labeled oligonucleotide. The resulting proximity yielded FRET-based quenching of the QD PL, allowing visual detection at clinically relevant concentrations of mucin 1, and from 250 nM to 10 μM via spectrofluorimetry. Similarly, Freeman et al. adopted a strategy based on the association of multiple nucleic acids strands for the detection of cocaine using a supramolecular aptamer assembly [115]. The aptamer was composed of two oligonucleotides that associated to form a binding pocket in the presence of cocaine. Although this structure was stabilized by Watson–Crick base-pairing, the complementarity was not sufficient to associate the two oligonucleotides in the absence of cocaine. One oligonucleotide was labeled with QD_{570}, and the other was labeled with Atto-590 dye. In the presence of cocaine, the supramolecular assembly provided the proximity for FRET. The decrease in QD PL was used as the analytical signal and the LOD for cocaine was 1 μM.

Liu et al. have developed an aggregative/dispersive method for the detection of cocaine and adenosine using aptamers as cross-linkers between Au NPs and QDs [116]. Each Au NP and QD was conjugated with an oligonucleotide probe that hybridized to different portions of an aptamer sequence. The resulting assembly and proximity between the QDs and Au NPs resulted in efficient quenching of the QD PL, as well as shift in the Au NP plasmon resonance. Subsequent introduction of target analyte and binding by the aptamer disrupted the Watson-Crick base-pairing between the aptamer and probe oligonucleotides. The aggregate dispersed, restoring the QD PL and Au NP plasmon resonance. Both changes in optical properties were used for detection. The latter was analogous to the seminal work of Elghanian et al. [117]. However, the advantage of using QDs was that a different emission colours could be associated with different aptamer linkages. The assembly of different and independent QD-Aptamer-Au NP aggregates was facilitated by the "chemical programmability" of Watson–Crick base-pairing. Multiplexed detection of adenosine and cocaine was demonstrated using QD_{525} and QD_{585}, respectively, in Au NP assemblies mediated by the corresponding aptamers. The LODs for cocaine and adenosine were 120 and 50 μM.

Although most QD-FRET bioprobes have, to date, been used for *in vitro* detection, their potential has been demonstrated in intracellular applications. In addition to the work of Freeman et al. with Nile Blue [105], Bagalkot et al. developed a bioprobe capable of targeting cancer cells and signaling drug delivery [118]. QD_{490} were modified with prostate specific membrane antigen-binding aptamer. Subsequent incubation with doxorubicin yielded QD-aptamer-doxorubicin conjugates via intercalation of the doxorubicin in the aptamer. Efficient energy transfer from the QDs to the doxorubicin largely quenched the QD PL. In turn, the doxorubicin emission was quenched due to the intercalation with the aptamer. The result was a dark bioprobe that selectively targeted prostate cancer cells and initiated uptake by endocytosis. The QD PL was restored after 1.5 h within the cells due to release of the doxorubicin (possibly by biodegradation). The cytotoxicity of doxorubicin towards the prostate cancer cells was unaffected by its delivery as a QD-aptamer-doxorubicin conjugate. In contrast, its cytotoxicity towards healthy cells was substantially decreased, indicating the efficacy of the targeting and release.

QDs have been adopted as donors in molecular beacons (MBs) and, analogous to MBs with fluorescent dye reporters, rely on hairpin opening and closing to modulate FRET. Studies by Kim et al. have demonstrated that, although QD-MBs can have lower signal-to-background ratios than conventional MBs, they have improved photostability and are capable of discriminating single nucleotide polymorphisms (SNPs) [64,119]. In addition to the QD-quencher spectral overlap, the QD-oligonucleotide linkage strategy was found to influence the signal-to-background ratio associated with QD-MBs [120]. Interestingly, Chen et al. found that QD-MB conjugates were much less susceptible to intracellular nuclease degradation [121]. The potential nuclease degradation of MBs or non-specific interactions that resulted in false-positive signals were identified to occur in the nucleus. In contrast to conventional MBs, the QD-MB conjugates were retained in the cytoplasm and minimal false positive signals were observed. This allowed measurement of oncogene expression in breast cancer cells. Although the above studies used dark quenchers as acceptors, QD-MBs with fluorescent acceptors have also been demonstrated [77].

In addition to MBs, FRET-based hybridization assays have been developed using the association of directly or indirectly labeled target with QD-probe conjugates. Direct labeling involves the covalent coupling of a fluorescent dye or dark quencher to target sequences. Indirect labeling can be achieved through a sandwich assay or the use of intercalating dyes sensitive to double-stranded nucleic acids. In a seminal contribution, the research group of Wang developed the use of QDs as donors in single-pair FRET spectroscopy for genetic analysis [65]. As illustrated in Fig. 3c, a sandwich format was used to avoid direct target labeling. QD_{605}-oligonucleotide probe conjugates and Cy5-labeled reporter oligonucleotides were designed to hybridize to adjacent regions of the target sequence. The resulting FRET-sensitized Cy5 fluorescence was used as the analytical signal. The 4.8 fM LOD was 100-fold better than dye-based MBs, and the utility of the bioprobe was further demonstrated in an oligonucleotide ligation assay to detect point mutations in clinical samples [65]. The same group later used QD-probe bioconjugates and FRET as a quantitative detection strategy for methylation specific polymerase chain reaction (MSP) [122]. In this case, Cy5-labeled primers were used to generate directly labeled targets via MSP. In contrast to conventional analysis methods, the QD-FRET bioprobe detection was single-step and only required as few as eight cycles of MSP (cf. 40 cycles). The simultaneous detection of two methylated sequences was possible using QD_{585}-Alexa Fluor 594 and QD_{585}-Cy5 FRET-pairs, where each acceptor dye was associated with different probe and primer sequences.

Our group initially looked at the development of multiplexed hybridization assays using QD_{526}-Cy3 and QD_{606}-Alexa Fluor 647 (A674) FRET-pairs [123]. The target oligonucleotides were directly labeled with the acceptor dyes, and different probes were associated with each QD donor. Hybridization generated the proximity required for FRET, and the ratios of donor-acceptor emission for each FRET-pair were used as the analytical signals. The respective LODs were 40 and 12 nM. This strategy provided the opportunity for the simultaneous detection of two target sequences in an ensemble using simple spectrofluorimetry (cf. single molecule spectroscopy), and without the use of multiple excitation sources, spatial registration (cf. microarrays), or sorting technology (cf. suspension arrays). Furthermore, the use of fluorescent acceptors permitted ratiometric analysis, which is more robust with respect to variations in sample composition and preparation. We further developed this strategy into multiplexed solid-phase hybridization assays, potentially capable of up to four-plex detection. These studies are cited and described in Section 4.

In our original solution-phase bioprobe, the challenge was the strong non-specific adsorption of oligonucleotides on mercaptoacetic acid (MAA) coated QDs [123,124]. This resulted in a high background signal from non-complementary sequences, long hybridization times, and a change in the thermodynamic stability of probe-target hybrids. The potential for false-positive signals from the adsorption of non-complementary sequences was overcome by the use of ethidium bromide (EB) as an acceptor dye. Since EB fluorescence is sensitive to double-stranded nucleic acid, adsorption did not strongly affect the observed signal. The disadvantage of the method was the high background fluorescence from non-

intercalated EB, where the associated LOD was 80 nM. However, this was offset by the ability to detect target even in the presence of a six-fold excess of non-complementary oligonucleotides, or a ten-fold excess of salmon sperm DNA. A hybridization assay that uses intercalated dyes as acceptors is illustrated in Fig. 3d and yields data similar to Fig. 4b,ii.

Zhou et al. also adopted the use of EB as an acceptor dye with QD_{553} in a hybridization assay [125]. In this case, non-specific adsorption was not an issue. Rather, the use of EB avoided direct labeling of target with Alexa Fluor 594. To avoid non-specific adsorption, these researchers coated the QDs with compact carboxy-terminated polyethylene glycol ligands. Similarly, Wu et al. also reported low non-specific binding in a hybridization assay using hydroxyl-terminated QD coatings [126]. These researchers used QD_{536}-Rhodamine Red (RhR) and QD_{589}-Texas Red FRET-pairs, but only in one-plex assay formats with directly labeled target. The LODs for the assays by Zhou et al. [125] and Wu et al. [126] were both in the nanomolar range. In addition, Bakalova et al. developed a hybridization assay for screening potential siRNA sequences against target mRNA [127]. This work was one of the earliest contributions to the field. Target mRNA was amplified and labeled by the polymerase chain reaction (PCR) using a Cy5-labeled nucleotide. Hybridization with QD_{580}-probe conjugates provided an analytical signal via FRET. This study found that the accessibility of the sense mRNA to the QD-conjugated antisense probe siRNA was important for hybridization efficiency. Optimization of linker length was necessary since the size of the QD hindered mRNA hybridization at short length linker lengths.

Recently, there have been several reports of QD–oligonucleotide conjugates assembled via electrostatic interactions. For example, Peng et al. used poly(diallyldimethylammonium chloride) (PDDA) to mediate the assembly of Cy3-labeled probe oligonucleotides on MAA-coated CdTe QD_{497} [128]. As an alternative to a cationic polymer, Lee et al. modified QD_{530} with a mixture of cationic and neutral PEG ligands to mediate the assembly of carboxytetramethylrhodamine (TAMRA)-labeled oligonucleotides [129]. In both cases, hybridization was signaled by a decrease in FRET efficiency. This was attributed to the increased rigidity of the probe-target duplex, resulting in an increase in donor–acceptor distance. Jiang et al. used a blue fluorescent cationic polymer to mediate the assembly of infrared dye-labeled probe-target duplexes on MAA-coated CdTe QD_{615} [130]. The fluorescent polymer was found to enhance the PL of the QD at excitation wavelengths shorter than ca. 400 nm. In this case, the difference in the strength of electrostatic attraction between double- and single-stranded nucleic acid provided contrast between target and non-complementary sequences, with the former providing larger FRET-sensitized infrared dye emission. Another "signal-on" approach was developed by Li et al., and relied on DNA adsorption on positively charged gold nanorods [131]. The hybridization of QD_{655}-labeled probes with target adsorbed on the gold nanorods resulted in PL quenching. The limitation in all these approaches has been substantial background from non-complementary sequences. Although such background is less than the signals observed with complementary target, the contrast ratio is generally small. As a consequence, these methods are not well suited to the analysis of samples when there is potentially a large background of non-complementary sequences.

Perhaps more so than in hybridization assays, the electrostatic assembly of nucleic acids and cationic polymers is important in the development of gene delivery strategies. The research groups of Wang and Leong have developed QD-FRET methods for investigating the electrostatic-driven condensation of DNA by cationic polymers [132–135]. These polyplexes are potential vectors for gene therapy, and optimization is necessary in order to avoid premature dissociation of the complex, or overly stable binding that prevents effective delivery. To obtain information about polyplex assemblies, plasmid DNA was biotinylated and conjugated with Streptavidin-coated QD_{605}. In turn, cationic polymers were labeled with Cy5, resulting in efficient FRET within the polyplex assemblies. This is illustrated in Fig. 3f. This system was used to characterize polyplexes incorporating chitosan, polyethyleneimine, and polyphosphoramidates. Through optical spectroscopy, microscopy, and SMD, it was possible to observe intracellular delivery and trafficking, as well as to quantitatively measure polyplex unpacking rates. These researchers also studied polyplex assembly kinetics using a microfluidic T-sensor [134]. The analytical signal was the evolution of FRET-sensitized Cy5 PL at the diffusion interface between two laminar flows – containing QD-labeled plasmid DNA and Cy5-labeld chitosan, respectively – in a microfluidic channel. In another study, QDs were conjugated to Cy3-labeled plasmid DNA, and assembled with Cy5-labeled cationic polymer [135]. When the polyplexes were intact, the energy transfer pathway was from QD_{525}-to-Cy3-to-Cy5. In this manner, it was possible to study two rate-limiting steps in gene delivery: the unpacking of the DNA polyplex, indicated by the loss of FRET-sensitized Cy5 PL; and nuclease degradation, indicated by the loss of FRET-sensitized Cy3 PL.

QD-FRET has also been used to develop *in vitro* assays for nuclease activity. The design was simply acceptor labeled nucleic acid that was conjugated to QDs to yield FRET. Nuclease activity cleaved the conjugate, and the loss of FRET was used as the analytical signal. Gill et al. [79] and Suzuki et al. [136] used this format to probe DNase activity. In the case of the latter, it was possible to combine the DNase probe with a second probe for trypsin activity. The FRET-pairs that were associated with the DNAase and the trypsin were spectrally resolved, and allowed simultaneous one-pot detection of nuclease and protease activity [136].

FRET-based QD probes for the detection of protease activity were initially reported by Chang et al. [137], Medintz et al. [138], and Shi et al. [139] in 2006. Conceptually, the design of these probes, and their successors, was analogous. Peptide sequences selectively cleaved by a target protease were labeled with an acceptor and assembled around a central QD donor, resulting in FRET-sensitized quenching of the QD PL. Proteolytic activity destroyed the proximity necessary for FRET, restoring the QD PL and providing an analytical signal. Target proteases have included: caspase-1 [138], caspase-3 [140,141], chymotrypsin [138], collagenase [137–139], matrix metalloproteinase-7 [141,142], thrombin [138,141], and trypsin [136,143]. In addition to proof-of-concept experiments for *in vitro* detection or protease activity or inhibition, the QD-FRET protease bioprobes have been used to measure extracellular matrix metalloproteinase (collagenase) activity between healthy and cancerous cells [139], and in enzyme inhibition screening assays to assess their potential in drug discovery [138]. The assays could be quantitative, with LODs as low as 20 pM (3.3 units). In addition, only small sample volumes (e.g. 7 μL on a microchip) and small amounts of substrate or enzyme were required for analyses [140,143].

Despite the similar underlying concept, there can be significantly different analytical performance between different QD-FRET protease bioprobe designs. For example, Chang et al. used peptide-conjugated Au NPs as an acceptor [137]. The average assembly of six peptide-Au NPs per CdSe/CdS QD_{620} resulted in 71% quenching of QD PL, and 52% was recovered after incubating 47 h with protease. A higher number of peptide-Au NPs per QD gave higher quenching efficiencies, but no PL recovery was observed. This observation, and the long assay time, was attributed to the size of the Au NPs (1.4 nm dia.) interfering with protease access to the peptide. In contrast, Medintz et al. [138] and Shi et al. [139] used Cy3 (QD_{538} donor), QSX-520 (QD_{522} donor), or RhR (QD_{545} donor) labeled peptides as an acceptor, and required analysis times of only 10–15 min. A

protease bioprobe using a peptide labeled with a fluorescent dye is shown in Fig. 3e and generates data similar to that in Fig. 4b,i. Recently, Boeneman et al. [140] and Suzuki et al. [136] have demonstrated QD-FRET protease detection using mCherry (QD_{550} donor) and Green Fluorescent Protein (QD_{490} donor) acceptors, respectively, assembled around QDs via peptide linkers. Assay times were ca. 30–90 min, suggesting that the slow enzyme velocity associated with Au NP acceptors was not strictly due to geometric size, but perhaps resulted from a combination of size and rigidity.

The slow proteolytic rate observed with Au NP acceptors [137] highlights the importance of considering the conformation of biomolecular probes conjugated to QDs. Medintz et al. recognized this in the design of their protease bioprobe [138]. To help ensure the QD-conjugated cleavage sequence was accessible to the protease, their peptide incorporated an alanine and α-aminoisobutyric acid rich sequence to act as a rigid helical linker between the substrate sequence and the polyhistidine sequence used for assembly on the QD. In most studies, peptide probes have been prepared and also labeled with an acceptor via chemical synthesis. However, an advantage of using fluorescent protein acceptors is that, through standard molecular biology techniques, the proteins can be expressed in bacteria with appended substrate peptide and polyhistdine sequences [140]. These constructs are ready to self-assemble on QDs, are inherently biocompatible, and no acceptor labeling steps are required.

Another important consideration in the design of QD-FRET protease bioprobes is the acceptor valence. Protease detection relies on a dissociative event and de-quenching of the QD PL. In practice, multiple acceptors (e.g. 2–6) are usually assembled on the QD to increase quenching efficiency according to Eq. (1). As shown in Fig. 2b, the FRET efficiency gradually reaches a plateau as the acceptor valence, *a*, increases. Mathematically, the largest *change* in FRET efficiency is observed between $a = 0$ and $a = 1$, and subsequently decreases with stepwise increases in *a*. However, the number of available biorecognition sites determines the upper limit of the dynamic range in any assay. A protease assay can be imagined as the counting of a series of discrete decreases in the number of acceptors across an ensemble of QD donors. Therefore, the acceptor–peptide conjugate valence should reflect a compromise between the optimal detection sensitivity associated with small values of *a*, and the larger dynamic range associated with large values of *a*. Working from experimentally measured FRET efficiency–acceptor valence curves, Medintz's research team has adopted the strategy of choosing a value of *a* such that the associated FRET efficiency is just prior to the plateau, as indicated by the asterisk in Fig. 2b [138,140,143].

Homogeneous immunoassays have also been developed using QD-FRET, and three different formats have been explored. Nikiforov and Beechem developed a competitive binding immunoassay for the detection of cortisol [144]. QD_{605} were conjugated with an estimated 12-15 cortisol molecules per QD. Anti-cortisol was labeled with A647 as an acceptor. The presence of cortisol in a sample decreased the formation of QD-cortisol/anti-cortisol-A647 complexes. The corresponding decrease in FRET was used as the analytical signal. As an alternative to a competitive binding assay, Wei et al. developed a sandwich assay (Fig. 3 g) for estrogen receptor β (ER-β) [57]. QD_{565}-labeled monoclonal anti-ER-β and Alexa Fluor 568-labeled polyclonal anti-ER-β were used to form the sandwich structure in the presence of ER-β, and to provide the necessary proximity for FRET. There were an average of seven Alexa Fluor 568 dye molecules per polyclonal antibody. Since the large size of immunoglobulins typically results in large donor-acceptor separations, the presence of multiple dye labels on an antibody can be important for maximizing FRET efficiency. The data was of the form shown in Fig. 4b,ii and the LOD of the ER-β assay was 0.05 nM. Stringer et al. employed a third immunoassay strategy that was unimolecular and relied on conformation changes upon antigen binding [145]. The target analyte was human cardiac troponin I (cTnI). QD_{544}-anti-cTnI conjugates were prepared using a protein A bridge. The protein A ensured the proper orientation of the anti-cTnI through self-assembly to the F_c region. The anti-cTnI was labeled with Alexa Fluor 546 dye to yield FRET. Upon binding of cTnI, a large conformational change in the anti-cTnI decreased the QD donor-dye acceptor separation. A corresponding increase in FRET-sensitized Alexa Fluor 546 emission provided the analytical signal, permitting detection in the range from 32 to 500 nM. The LOD increased to 55 nM with blood plasma as a sample matrix. It should also be noted that Goldman et al. developed a competitive binding immunoassay for a non-biological target, trinitrotoluene, using QDs as donors in FRET [56].

3.2. Bioluminescence energy transfer

3.2.1. BRET and QDs

A conventional FRET experiment uses optical excitation to create an excited state donor that is capable of transferring energy to a ground state acceptor. In contrast, chemiluminescence and bioluminescence resonance energy transfer (CRET and BRET, respectively) generate an excited state donor through a chemical reaction. The distinction between CRET and BRET is that a biochemical reaction is the basis of the latter. In both cases, once an excited state donor is produced by a chemical reaction, the efficiency of energy transfer can be modeled using the conventional FRET formalism.

An advantage of CRET and BRET over FRET is very low background, even in complex samples. The absence of optical excitation avoids sample autofluorescence, strong scattering of source light, and spurious acceptor emission from direct excitation. As indicated in Section 3.1.1, the latter is a particular challenge with QDs due to the inability to avoid efficient direct excitation. In contrast, QDs are ideal energy acceptors in CRET and BRET due to their strong broad absorption that enables potentially large spectral overlap integrals, and excellent spectral separation between donor and acceptor emission. The preparation of QD-enzyme conjugates allows chemiluminescent and bioluminescent reactions to be localized to the surface of QDs, providing the proximity required for CRET or BRET. Although QDs have been studied as acceptors in CRET [146,147], more progress has been reported in bioprobe development using QDs as acceptors in BRET.

To date, the bioluminescent system of choice has been the *Renilla* luciferase enzyme (Rluc) and its substrate coelenterazine. Bioluminescence arises from the conversion of coelenterazine (a luciferin) into excited state coelenteramide by oxidative decarboxylation. Long-lived light-emission kinetics and ATP insensitivity are advantages of the Rluc system. Coelenteramide emission is broad, and spans the blue-green region of the visible spectrum with a maximum at ca. 480–485 nm. As shown in Fig. 5b, the emission spectra of QDs with peak PL at wavelengths longer than approximately 625 nm are completely resolved from the Rluc emission, and good spectral overlap between the Rluc emission and QD absorption is obtained.

3.2.2. Applications

This section highlights the development of assays and bioprobes based on QDs as acceptors in BRET. Although not yet as widely employed as FRET methods, the popularity of BRET methods continues to increase. A recent review has highlighted the growth and development of luciferases and bioluminescent proteins in analytical applications, without specific emphasis on QDs [148]. Table 1 lists and categorizes the examples cited below.

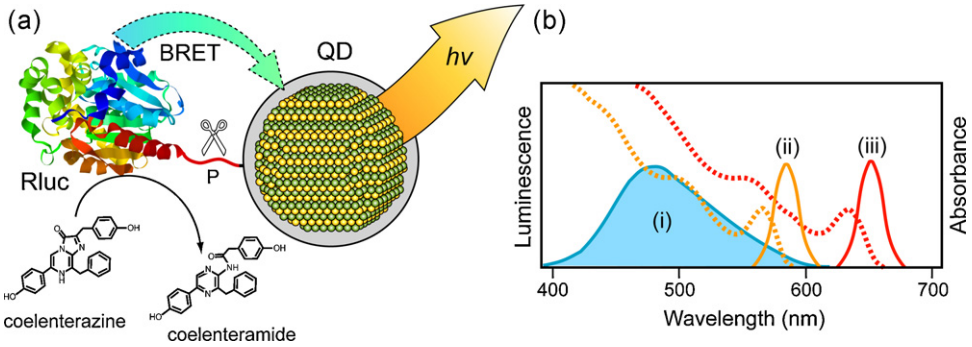

Fig. 5. (a) QD-BRET construct for the detection of protease activity [80,87]. The conversion of coelenterazine to coelenteramide by *Renilla* luciferase (Rluc) drives energy transfer to the QD, which acts as an acceptor. The "BRET arrow" from the Rluc is for illustrative purposes. The donor is actually excited state coelenteramide localized at the Rluc. The Rluc is coupled to the QD by a peptide sequence (P) that is selectively cleaved by the target protease (scissors). A monovalent conjugate is shown for simplicity. Figure not to scale. The general form of the experimental data associated with this system is illustrated in Fig. 4d. (b) The qualitative spectral overlap between (i) coelenteramide emission, and the absorption of (ii) yellow or (iii) red emitting QDs (dashed lines). Nearly the entire emission spectrum of coelenteramide overlaps with the QD absorption (blue shaded region) . The corresponding emission spectra of the QDs are shown as solid lines.

Cissell et al. developed a competitive binding assay for the selective detection of nucleic acids using Rluc as a BRET donor for QD_{710} [149]. A probe complementary to the target sequence was conjugated to the QD. The Rluc was conjugated to a competitor with the same sequence as the target. In the absence of target, hybridization between the probe and competitor created the proximity required for BRET. Unlabeled target in the sample also hybridized with probe, but without associated BRET. The analytical parameter was the ratio of donor-to-acceptor emission, and increased as the amount of target increased relative to the competitor. The LOD was 20 nM, and the assay was functional in cell extract.

The research group of Rao has received much attention for their development of self-illuminating QDs for biological imaging [150,151]. The self-illumination was a result of BRET between Rluc and QDs as bioconjugates. This group has also extended their QD-Rluc bioconjugates to the development of bioprobes for protease activity. In one study, a polyhistidine appended peptide substrate for matrix metalloproteinase-2 (MMP-2) was genetically fused to the C-terminus of an Rluc mutant [80]. The polyhistidine tail allowed conjugation to a carboxylate coated QD_{655} via bridging Ni^{2+} ions, creating the proximity required for efficient BRET (Fig. 5a). Hydrolysis of the peptide substrate by MMP-2 removed the proximity, and protease activity was measured via the decrease in the ratio of QD-to-Rluc emission (Fig. 4d). The LOD was 2 ng mL^{-1} with 24 h incubation. The assay had good selectivity when tested against MMP-7 and AcTEV proteases. In a second study, a different method was used for the preparation of QD-Rluc bioconjugates [87]. Hydrazide functionalized QD_{655} were conjugated with an Rluc-MMP-7 substrate fusion protein via intein-mediated chemical ligation. The ratio of QD-to-Rluc emission had a log-linear dependence on MMP-7 concentration, and the LOD for a 1 h assay was 5 ng mL^{-1}. The assay also functioned in serum, and was tested on cancer cell secretions. Multiplexed detection of MMP-2 and urokinase plasminogen activator was possible by preparing Rluc fusion proteins with the corresponding peptide sequences for cleavage sites. Conjugation of the Rluc proteins to QD_{655} and QD_{705}, respectively, provided two channels of detection based on BRET-sensitized acceptor QD emission.

The broad emission of the Rluc suggests that, with spectral deconvolution, the maximum multiplexing capacity of the BRET assays will be 3–4 acceptor QDs (and associated proteases). The disadvantage of introducing overlap between QD emission spectra to achieve higher order multiplexing is that the LOD will increase due to uncertainty in deconvoluting small changes in QD PL. Nonetheless, QD-BRET is very promising for *in vitro* and potentially *ex vivo* or *in vivo* protease detection.

3.3. Charge transfer quenching

3.3.1. Charge transfer and QDs

The optical excitation of QDs results in the formation of a bound electron–hole pair called an exciton. To generate efficient PL, the rate of radiative recombination of the exciton must be competitive with the rates non-radiative recombination processes. One such non-radiative process is Auger recombination, where the excited state energy is transferred to another carrier rather than lost as an emitted photon. Due to confinement within the nanocrystal, there is a very strong Coulomb interaction between an exciton and an "extra" carrier. As a result, the rate of Auger recombination in ionized QDs is many orders of magnitude larger than radiative recombination and PL is quenched [152]. Therefore, CT reactions between QDs and other redox active species provide a mechanism for the on/off switching of PL, and thus a basis for the design of bioprobes and biosensors.

The initial development of sensors based on CT quenching can be traced back decades. Fluorescent photoinduced electron transfer (PET) sensors for ions have been widely reported in the literature [153,154]. These sensors are constructed using a fluorophore-spacer-receptor architecture. Electron transfer from the receptor to the fluorophore drives PL quenching upon photoexcitation of the latter. Ion binding at the receptor shifts the energy of the receptor molecular orbitals and PET is no longer energetically favourable, thereby restoring the PL of the system. According to theory, the rate of electron transfer, k_{et}, is given by Eq. (3), where: V_o is the donor–acceptor electronic coupling at r_o, the van der Waals separation; r is the actual separation; β is a parameter that determines the decrease in coupling with distance; λ is the reorganization energy; and ΔG° is the standard free energy change for the CT reaction [155–157].

$$k_{et} = \frac{2V_\circ^2}{h} \exp\left[-\beta(r - r_\circ)\right] \left(\frac{\pi^3}{4\lambda RT}\right)^{1/2} \exp\left[-\frac{(\Delta G^\circ + \lambda)^2}{4\lambda RT}\right] \quad (3)$$

Thus, in the case of PET sensors, transduction is achieved by altering the free energy term in Eq. (3). This strategy has been successfully demonstrated for ion sensing using QD-spacer-receptor constructs [158,159], and more details are given in Section 3.3.2. However, transduction by alteration of the free energy term in Eq. (3) is not convenient when considering biomolecule targets. However, from Eq. (3), it is also observed that CT reactions have an exponential dependence on donor–acceptor separation. Indeed, in a system with ferrocene conjugated to QD_{605} via alkyl tethers of different lengths, the PL quenching efficiency associated

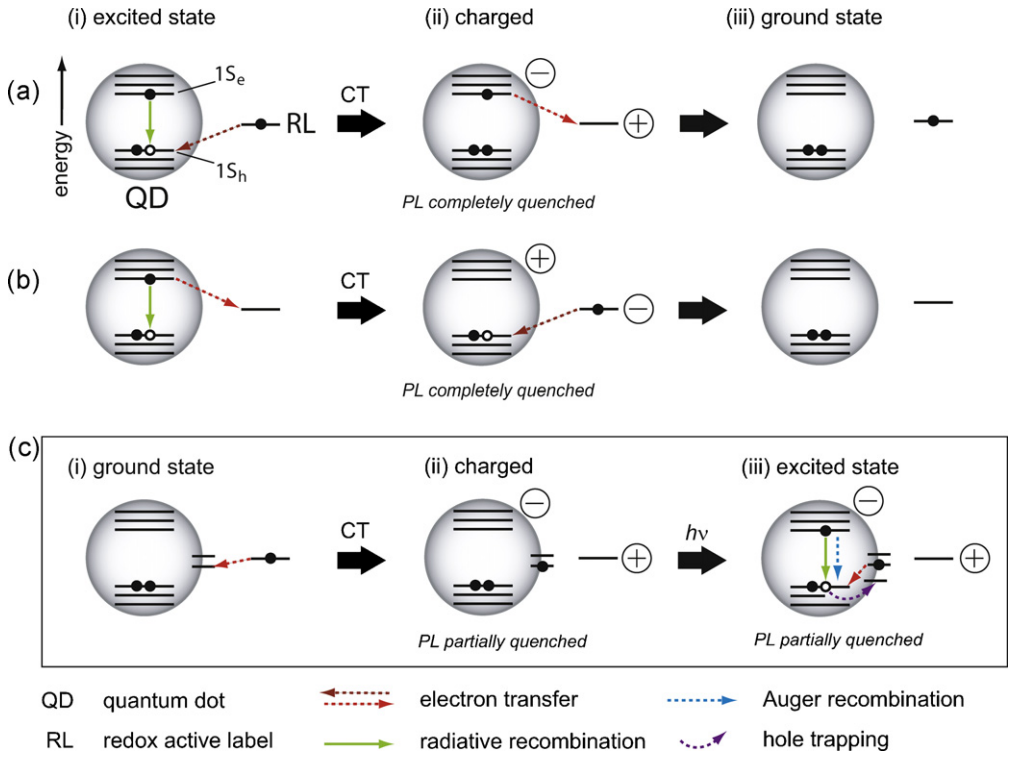

Fig. 6. Potential mechanisms of charge transfer quenching of QD PL. (a) Photoinduced hole transfer from (i) an excited state QD to a proximal redox label results in (ii) a non-luminescent ionized QD. Subsequent electron transfer to the redox label can regenerate (iii) a neutral, ground state QD. (b) Photoinduced electron transfer from (i) an excited state QD to a proximal redox label results in (ii) a non-luminescent ionized QD. Subsequent hole transfer to the redox label can regenerate (iii) a neutral, ground state QD. The mechanisms in (a) and (b) provide non-radiative relaxation pathways that compete with radiative recombination of the exciton. However, (a) and (b) only consider the core states of the QD. (c) Charge can also potentially (i) transfer to the surface states of ground state QDs to yield (ii) an ionized QD where the PL is not completely quenched. Upon (iii) photoexcitation, the non-radiative pathways that compete with radiative recombination of the exciton potentially include: Auger recombination, hole trapping, and electron transfer to core states.

with photoinduced CT was observed to decrease as the tether length increased [160]. Changes in donor–acceptor distance have been used to modulate PL quenching efficiency for the transduction of biorecognition events in two ways: (1) the association and dissociation of redox active labels at the surface of a QD; and (2) binding-induced conformational changes in redox-labeled biomolecules. The strong distance dependence of CT is particularly advantageous for latter, and provides more sensitivity to small changes in distance when compared to FRET. In contrast to the molecular fluorophores used in PET sensors, QDs provide a large interface for CT reactions. Multiple redox active species can be arrayed around the QD to improve CT efficiency [161]. In combination with their unique optical properties, the ability of QDs to serve as a scaffold has provided new opportunities in the development of CT-based optical bioprobes and biosensors.

The process of CT reactions involving QDs is not, to a first approximation, significantly different than that involving only molecules or ions. Most chemists are comfortable considering CT reactions within a molecular orbital framework, and this is also a good intuitive approach with QDs. The electronic structure of a QD is characterized by the size-dependent transition of the bulk conduction band (CB) and valence band (VB) into discrete states or "quantum confined orbitals" at nanometer dimensions. The lowest energy excitation (first exciton peak) corresponds to an electron in the $1S_e$ state (CB) and a hole in the $1S_h$ state (VB). Photoinduced CT reactions are associated with the introduction of a state that is intermediate in energy relative to the $1S_h$ and $1S_e$ states of the QD. The molecular orbitals of proximal redox active species are able to physically add these states through overlap with the electron or hole wavefunctions of the QD. As a result, CT becomes a competitive pathway with the radiative recombination of excitons. For example, as shown in Fig. 6a, following optical excitation of the QD, an electron can transfer from the $1S_e$ state to an empty intermediate energy state. Alternatively, a hole can transfer from the $1S_h$ state to an occupied intermediate energy state as shown in Fig. 6b. In both cases, these intermediate states are localized outside the core nanocrystal, resulting in separation of the carriers and ionization of the QD. The QD PL remains quenched until the charge on the QD is neutralized. The reorganization energy associated with these processes has not yet been determined, but is expected to be small due to the delocalization of the carriers in QDs [162]. In many cases, it has been suggested that rapid CT from the proximal redox active species back to the QD can occur, and that the QD is only transiently ionized [163,164]. This is ideal for the development sensors, where rapid recovery of QD PL is desired. However, it should be noted that hole trapping has been suggested as the cause of slow neutralization times (~μs) following PET from a CdSe QD_{500} to an adsorbed Rhodamine B molecule [162]. Slow neutralization of QD charge has also been implicated in the blinking of single QDs [26,152].

The discussion thus far has neglected that surface states are an important feature of the electronic structure of QDs. Recently, Medintz et al. have demonstrated that proximal ruthenium phenanthroline complexes were able transfer charge into both QD_{590} core states (e.g. VB) and surface states [161]. In the case of the latter, the CT was independent of optical excitation. Similarly, Shim et al. have previously observed spontaneous CT into the CB and surface states of CdSe or CdSe/ZnS QD_{590} using a strong reducing agent [165]. Furthermore, as described later in this review, the importance of QD surface states in CT reactions occurring at electrodes has been recognized in ECL experiments. Medintz et al. found that the ligand coating on the QDs was important in determining if the core and surface states were involved in CT [161]. In partic-

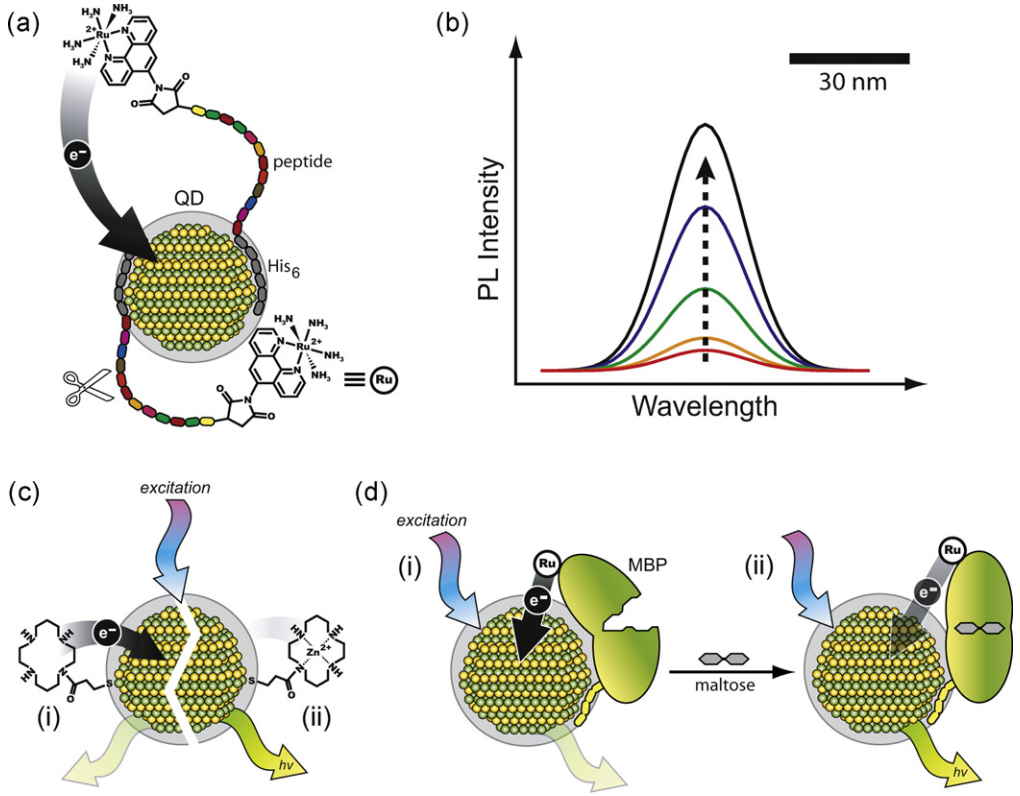

Fig. 7. (a) QD-CT construct for the detection of protease activity [161]. Ruthenium phenanthroline labeled peptides are conjugated to QDs via a polyhistidine tag. The peptide ruthenium-QD proximity in the bioconjguate is sufficient for CT quenching of the QD PL. Protease activity (scissors) cleaves the ruthenium phenanthroline from the QD, restoring PL (not shown). (b) The recovery of the QD PL in response to increasing protease activity (direction of the dashed arrow) in part (a) of the figure provides an analytical signal. This basic form of experimental data is also characteristic of the constructs in parts (c) and (d). (c) The detection of zinc ions using Cyclam-conjugated QDs [159]. (i) In the absence of zinc, efficient CT between the Cyclam and QD largely quenches the QD PL. (ii) After zinc binding, the CT is inhibited and the QD PL is restored. (d) A unimolecular QD-CT sensor for the detection of maltose [163,174]. Maltose binding protein (MBP) site-specifically labeled with ruthenium phenanthroline is assembled on a QD via a metallothionein tag. (i) The proximity between the ruthenium label and the QD is sufficient for CT quenching of the PL. (ii) A conformational change in the MBP after binding maltose increases the QD-ruthenium separation, partially restoring the QD PL. Figures not to scale.

ular, the charge of the ligand was suggested to play a role, where CT occurred to both the VB and surface states of neutral DHLA-PEG coated QDs, but only to the surface states of anionic DHLA coated QDs. Regardless of ligand, the quenching efficiency decreased with increasing core size—an observation that could potentially be due to a higher density of surface states in smaller QDs [161].

In contrast to adding charge to VB or CB states, the addition of charge to surfaces states does not necessarily cause complete quenching of PL. The interaction of an exciton with a carrier localized at the QD surface is much less than that with a carrier localized within the core, and radiative recombination remains a competitive relaxation pathway [161]. The result is only partial PL quenching. Moreover, greater carrier overlap in smaller QDs is another potential cause of the higher quenching efficiency observed with smaller QDs by Medintz et al. [161]. From Eq. (3), the rate of CT should depend on QD size. The energies of the CB and VB states scale with core size, and therefore alter the free energy change associated with CT. Indeed, Robel et al. have observed the effect of QD size on CT rates between QDs and TiO_2 particles [166]. Nonetheless, additional studies are required to elucidate the size-dependence of CT quenching. It is important to examine the quenching efficiency across a series of QD sizes, across different QD materials, and at controlled valences of different proximal redox species.

The importance of surface states adds a further level of complexity in understanding the CT quenching mechanisms of QD-redox label conjugate systems. As illustrated in Fig. 6c, surface states could potentially be intermediates in CT between proximal states and the core states. If surface states can be ignored, then the relative rates of radiative exciton recombination and CT to core states determine the efficiency of PL quenching. In contrast, if surface states are important, there are two new rates to potentially consider: the enhancement of non-radiative rates due to the added surface charge (e.g. Auger recombination or hole trapping [165]), and the rate of CT from surface states to core states. In either case, efficient neutralization of the QDs and regeneration of the redox label are analytically important for reliable equilibrium measurements in sensing experiments.

It is clear that further study is needed to elucidate the nature of CT processes involving QD-redox label conjugates, and several analytical tools are suitable for this research. The occupation of electronic states can be determined using steady-state and transient absorption spectroscopy, in both the visible (inter-band transitions) and infrared regions (intra-band transitions) of the spectrum [161,162,165–167]. The combination of steady-state and time-resolved PL spectroscopy can elucidate quenching mechanisms. Cyclic voltammetry is useful in characterizing the states involved in electron transfer [161,168–171], and electron paramagnetic resonance (EPR) spectroscopy can be used to identify radicals [172,173]. Although there is need for further study, several bioprobes and biosensors have been developed using QDs and CT quenching of PL. These are summarized in the next section, categorized in Table 1, and selected examples are illustrated in Fig. 7.

3.3.2. Applications

The Benson group has developed several unimolecular biosensors using CT quenching and QD-protein conjugates labeled with ruthenium complexes [163,174–177]. Unimolecular sensors are reagentless, potentially allow regeneration and continuous

measurements without immobilization, and are not subject to dilution-driven loss of a quencher or reporter species (cf. bimolecular constructs). Unimolecular constructs have been developed for sensing maltose, lead, thrombin, and fatty acids.

Prototype unimolecular CT biosensors were initially developed using both CdSe [174] and CdSe/ZnS [163] QDs conjugated with maltose binding protein (MBP). The MBP was appended with a C-terminal metallothionein domain for assembly on the QD, and surface cysteine residues were used for the site-specific attachment of a ruthenium complex. The introduction of a proximal ruthenium complex via MBP quenched the PL of CdSe/ZnS QD_{565} up to 22%. The binding of maltose by MBP induced a conformation change in the protein that increased the distance between the ruthenium complex and the QD, largely restoring the QD PL to its unquenched intensity. Fig. 7c illustrates this method of transduction. The selectivity of the sensors was tested against several sugars. The response to maltose was a $22 \pm 3\%$ increase in PL. Of the other sugars, only L-mannose increased the PL, and by a much smaller $3 \pm 2\%$. Reversible sensing was demonstrated by the addition of α-glucosidase. An analogous construct was developed for the detection of lead at nanomolar levels in red blood cell solutions [175]. Metalloprotein design was used to re-engineer phosphate binding protein for the selective binding of lead (PBP-Pb^{2+}), and subsequent conjugation to CdSe/ZnS QD_{545} or InGaP/ZnS QD_{660}. In the case of the latter, lead binding caused a 45–75% decrease in QD PL, suggesting a decrease in the QD-ruthenium separation upon a protein conformational change that was induced by selective binding. For both the MBP and PBP-Pb^{2+} constructs, the mechanism of quenching was suggested to be PET from the proximal ruthenium complex to the QD VB.

In addition to protein conformational changes, the Benson group has demonstrated the potential for a sensing construct based on CT quenching modulated by protein binding pocket solvent occupancy [176]. The binding of palmitate in a hydrophobic pocket of intestinal fatty acid binding protein causes a significant change in the solvent occupancy of the binding pocket. The introduction of a ruthenium label in the pocket allowed transduction via CT quenching. Desolvation upon palmitate binding increased the rate of CT between the QD_{565} and ruthenium complex, decreasing the QD PL by 32–58%. This could have been due to changes in the reorganization energy and β terms in Eq. (3). The quenching efficiencies are comparable to those driven by conformational changes, suggesting two feasible routes to developing sensing constructs. Given that changes in conformation and changes in solvation are often both associated with protein–ligand binding, tuning the superposition of these two effects may provide a means for signal optimization.

A QD-CT construct for sensing thrombin has also been developed by the Benson group [177]. Instead of protein conformational changes, a double-stranded oligonucleotide incorporating the TBA sequence was designed to modulate the distance between QD_{545} and ruthenium phenanthroline labels. The double-stranded structure was coordinated to the QD at one terminus by a thiol modification. The opposite terminus was labeled with a ruthenium complex. Upon thrombin binding, the furthest portion of the double helix, corresponding to the TBA sequence, was unwound. This decreased the QD-ruthenium complex separation and increased the CT quenching efficiency, enabling transduction. Tuning of the QD coating was required to avoid non-specific interactions and aggregation, while control of conjugate valence was important in determining the direction and magnitude of the observed PL changes. Due to steric effects, a 5:1 ruthenium-oligonucleotide-QD conjugate exhibited a PL enhancement of 50% at high thrombin concentrations, while a 1:1 conjugate exhibited a 30% decrease. Differences in thrombin binding isotherms were also observed across different systems. The work of the Benson group, and particularly this study, demonstrate that although the modulation of CT quenching through biomolecule conformational changes is widely applicable to developing biosensors, it is not necessarily straightforward. The *a priori* design of a construct may subsequently require extensive optimization through experiment before effective sensing can be realized.

In contrast to the sensors developed by the Benson group, which rely on small changes in QD-redox label separation, several bioprobes have been developed using the association or dissociation of redox active labels at the QD surface. For example, Yildiz et al. provided one of the earliest examples of this approach by developing a model assay based on the biotin-Streptavidin interaction [178]. The electrostatic assembly of a biotinylated derivative of methyl viologen (a bipyridinium dication) on MAA-coated QD_{563} caused significant quenching of the QD PL. This was attributed to PET from the QD to the methyl viologen. The QD PL was restored by the introduction of Streptavidin, which tightly bound the biotinylated methyl viologen and disrupted its interaction with the QD.

Medintz et al. have explored the detection of protease activity using peptides appended with ruthenium phenanthroline [161,179]. Peptide sequences recognized by the enzymes chymotrypsin and thrombin were conjugated to QD_{540} and QD_{590}, respectively, via a terminal hexahistidine tag [161]. A ruthenium phenanthroline maleimide label was introduced using a cysteine residue at the opposite terminus of each peptide (Fig. 7a). PL quenching exhibited a strong dependence on the number of ruthenium complexes conjugated to the QD. PL losses of 80% and 70% were observed with 1.5 thrombin substrates per QD_{540}, and 4.0 chymotrypsin substrates per QD_{590}, respectively. The difference in conjugate valence to achieve similar magnitudes of PL quenching was attributed to more efficient quenching of smaller sized QDs associated with the thrombin peptide. The introduction of increasing concentrations of thrombin or chymotrypsin gradually restored the corresponding QD PL through cleavage of the peptide tethers, removing the proximity required for CT. Enzyme reaction velocities and Michaelis–Menten constants were measured and found to be similar to those obtained in analogous FRET-based sensors [138]. The measurement of enzyme inhibition was also possible. In a second study, these researchers further demonstrated that QD–peptide–ruthenium conjugates are well suited for multiplexed analyses [179]. Mixed populations of four, six, and eight colours of $QD_{510/537/555/565/581/590/610/635}$ were prepared, where selected colours of QD were conjugated with ruthenium labeled peptides to drive PL quenching. The PL spectra of the mixtures (similar to Fig. 4e) were deconvoluted using a superposition of Gaussian peak shapes to quantitatively resolve the quenching of individual colours of QDs. This potentiates future development of a nano-scale suspension array, where each colour of QD is conjugated to a different peptide substrate to simultaneously monitor the activity of up to eight proteases. The advantage of using this method over FRET is the larger multiplexing capacity. FRET is limited by the number pairs that can be fit in a given wavelength range, and the requirement for spectral overlap. This is further compounded in QD systems where fluorescent acceptors are used, requiring more demanding deconvolution for similar levels of multiplexing. In contrast, ruthenium appears to have the potential to act as a "broadband" or "universal" quencher of QD PL in multiplexed assays. The Gaussian peak shape associated with QD PL also allows straightforward deconvolution and better confidence in analyses.

Gill et al. developed a QD-CT bioprobe suitable for the detection of tyrosinase and thrombin activity [180]. CdSe/CdS/ZnS multishell QD_{600} were conjugated with either tyrosine methyl ester or a peptide terminated with a tyrosine residue. In the case of the latter, the peptide sequence was selectively cleaved by thrombin. In both cases, the activity of tyrosinase converted the tyrosine to an *o*-quinone derivative that quenched QD PL by CT, providing the analytical signal. In the case of the peptide conjugate, thrombin activity

cleaved the *o*-quinone labeled peptide from the QD and restored its PL. In addition to the detection of tyrosinase activity, this method may also be useful for the enzymatic introduction of redox active labels on biomolecules (cf. ruthenium phenanthroline maleimide).

The development of QD-CT quenching bioprobes and biosensors is not limited to the use of biological molecules as affinity probes. In addition to the work on Benson [175], Ruedas-Rama and Hall have developed QD probes for the selective detection of biologically relevant ions using CT quenching [158,159,164]. The selective binding of ions by macrocycles or other chelating agents was used to alter photoinduced CT quenching of the QD. It should be stressed that, in these applications, CT between the QD and bound analyte ion did not provide the basis for transduction. Instead, the binding of the ion altered the CT quenching pathway between the macrocycle/chelating agent and the QD, where the former was conjugated to the QD. For example, a zinc sensor was constructed from QD_{620} by conjugation with an azamacrocycle using an amide linkage [159]. In the absence of zinc, the conjugated azamacrocycles quenched the QD PL (ca. 80–97%) by photoinduced hole transfer (i.e. PET to the valence band of the QD). The addition of zinc and subsequent binding blocked the CT quenching pathway by locking up the associated electron(s) in coordination to the metal ion. The resulting increase in QD PL was proportional to the concentration of zinc. Fig. 7b illustrates this transduction method. The azamacrocycles cyclam and cyclen provided LODs of ca. 1–2 μM, linear response over two orders of magnitude, and relative standard deviations of approximately 3%. Good selectivity was observed against other physiologically prevalent cations, and regeneration of the zinc sensor was possible with the addition of the ethylenediaminetetraacetic acid (EDTA). Furthermore, the detection of zinc was possible in the presence of calf fetal serum and Dulbecco's modified Eagle's medium—the latter is used to mimic intracellular environments.

In a similar strategy, the detection of manganese was possible using Zincon (2-carboxyl-2-hydroxy-5-sulfoformazylbenzene) assembled on negatively charged MPA-coated $QD_{500/540/620}$ using a layer-by-layer approach [158]. The positively charged polymer, poly(allylamine hydrochloride) was used to mediate assembly. Quenching of the QD PL (ca. 75%) by Zincon was attributed to photoinduced hole transfer from the QD. Disruption of the CT pathway by the Zincon–manganese interaction provided a basis for transduction by QD PL recovery analogous to the azamacrocycle zinc sensor above. A particularly important aspect of this study was the observation that multiple relaxation pathways may be superimposed on the same system. Many metal-ligand complex ions can have strong absorption and non-trivial fluorescence quantum yields. Proximal interactions may therefore potentially include both CT and FRET. In contrast to manganese, the Zincon–QD conjugate PL was further quenched by the addition of zinc ion. This was attributed to strong spectral overlap between the QD PL and the absorption of the zinc–Zincon complex, resulting in FRET. In contrast, isolated Zincon, and the manganese–Zincon complex, did not have significant spectral overlap with the QDs used. Ruedas-Rama and Hall have also studied a system where both CT and spin–orbit coupling were potential mechanisms of QD PL quenching [164]. Lucigenin, an acridinium dication dye sensitive to chloride, was conjugated to QDs and provided a basis for a chloride sensor via changes in QD PL. Although the relative importance of the two possible quenching mechanisms was not resolved, the study further highlights that the net interaction between a QD and proximal chromophores, fluorophores, or redox active species may potentially be a superposition of multiple interactions.

In addition to *in vitro* applications, Clarke et al. demonstrated the potential for the intracellular application of QD bioprobes based on CT quenching [181]. Dopamine–QD_{560} conjugates were prepared and used as a redox-sensitive luminescent stain for cellular imaging. Under reducing conditions, QD PL was visible in the peripheral regions of the cell and within lysosomes. Under highly oxidizing conditions, the QD PL was visible throughout the cell. In less severe oxidizing conditions, the mitochondria and perinuclear region of the cell were labeled. The cellular redox conditions were generated by the enhancement or suppression of glutathione synthesis, suggesting further application of these conjugates as a bioprobe for glutathione.

3.4. Electrochemiluminescence

An electrochemiluminescence (ECL) experiment typically beings with stable precursors that are converted to reactive species at the surface of an electrode under an applied potential. The resulting intermediates can undergo CT reactions to form an excited state product that relaxes via luminescence. As a combination of electrochemistry and optical spectroscopy, ECL provides several potential advantages. The electrochemical initiation of the luminescent reaction offers temporal and spatial (localized to electrode surface) control, while the absence of optical excitation avoids background from scattered source light or sample autofluorescence. However, because luminescence is the analytical parameter (not electrical current), the method is much less susceptible to many of the interferences associated with voltammetric methods. Multi-parameter analyses are possible using ECL onset or peak voltages, ECL intensity, and wavelength. The interested reader can find further details on ECL and its applications in two excellent reviews [182,183].

3.4.1. Electrochemiluminescence and QDs

The ECL of several different QD materials has been studied [184–191]. Although the details are too extensive to review here, there are several observations of analytical interest. Foremost, QDs support ECL with or without a coreactant. In the case of the former, anodic and cathodic potentials are cycled at an electrode to create oxidized (hole injected) and reduced (electron injected) QD species, respectively. As shown in Eqs. (4)–(6), the oxidized and reduced QD species can react in the electrode diffusion layer, producing an excited state (QD^*) that can relax via luminescence. The oxidized and reduced QD species are not necessarily stable, and scan rate is important in optimizing ECL intensity. Depending on the QD material, the oxidized (e.g. Si, CdSe) or reduced (e.g. Ge) species may be more stable than its counterpart.

$$QD + e^- \rightarrow QD^- \quad (4)$$

$$QD + h^+ \rightarrow QD^+ \quad (5)$$

$$QD^- + QD^+ \rightarrow QD^* + QD \quad (6)$$

In the coreactant mechanism, and considering cathodic ECL, both the QD (Eq. (7)) and a second molecular species (i.e. the coreactant) are reduced at the working electrode. The coreactant is reduced to a strong oxidizing agent (Eq. (8)), which can inject a hole into a QD species (Eq. (9)). Analogous to Eq. (6), an excited state QD can be produced by the reaction between a reduced QD and a QD oxidized by the coreactant, or also by the direct injection of a hole into a reduced QD by the coreactant (Eq. (10)). A common example of a coreactant for cathodic ECL is the peroxydisulfate anion, which reacts via Eqs. (8)–(10). Fig. 8a illustrates Eqs. (7), (8) and (10).

$$QD + e^- \rightarrow QD^- \quad (7)$$

$$S_2O_8^{2-} + e^- \rightarrow SO_4^{2-} + SO_4^{\bullet -} \quad (8)$$

$$SO_4^{\bullet -} + QD \rightarrow SO_4^{2-} + QD^+ \quad (9)$$

$$QD^- + SO_4^{\bullet -} \rightarrow QD^* + SO_4^{2-} \quad (10)$$

Poznyak et al. have observed the cathodic charging of the lowest unoccupied CB quantum confined state ($1S_e$) via the bleach

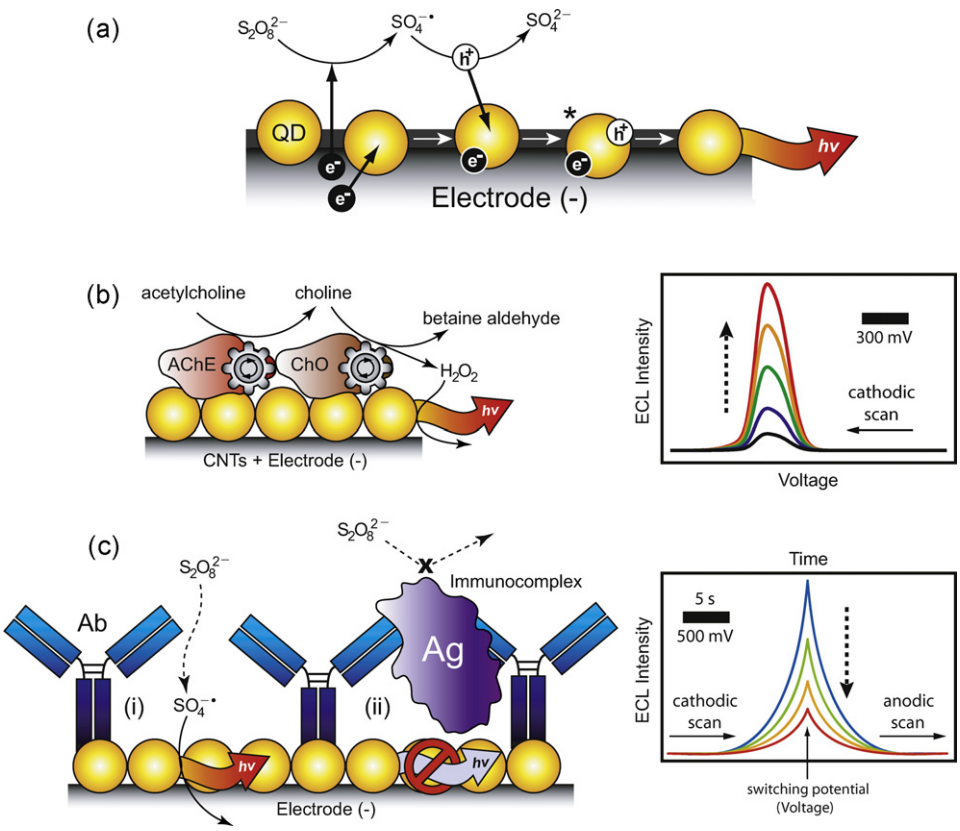

Fig. 8. (a) Illustration of the cathodic ECL mechanism using peroxydisulfate as a coreactant. (b) Acetylcholine detection using QDs and cathodic ECL (CNTs not shown) [200]. The combined catalytic activity of acetylcholine esterase and choline oxidase produces hydrogen peroxide as a byproduct. Hydrogen peroxide is an efficient ECL coreactant and the ECL intensity is proportional to the amount of acetylcholine. The basic form of the experimental data is illustrated and shows the increase in ECL intensity with increasing acetylcholine or choline concentration (direction of the dashed arrow). (c) A general strategy for immunosensing using QDs, antibodies (Ab), and cathodic ECL [201–204]. Compared to the absence of antigen (Ag) in (i), the presence of antigen and the formation of an immunocomplex in (ii) increases CT resistance, and decreases ECL intensity. The CT resistance increases due to occlusion of the electrode surface by the immunocomplex. The basic form of the experimental data is illustrated and shows the decrease in ELC intensity with increasing concentration of antigen (direction of the dashed arrow). Figures not to scale. Further details can be found in the main text.

of the first exciton absorbance [192]. In experiments using peroxydisulfate as a coreactant, these authors also coined the term "quantum confined cathodic protection" to describe the efficient $1S_e$–$1S_h$ radiative recombination, in preference to further oxidative corrosion, following hole injection into the corresponding VB state by the sulfate radical anion.

It is also important to note that QD-ECL is very sensitive to the surface states. For example, the QD-ECL first observed from Si and CdSe QDs originated from band-gap states [175,185]. In contrast, the ECL observed in an analogous experiment with CdSe/ZnS was largely associated with band-edge luminescence [186]. In this case, the shift from dominant band-gap to band-edge luminescence was attributed to the ZnS passivation of surface traps states. However, band-edge ECL has also been observed with CdSe, CdTe and Ge QDs lacking shell structures [187,188,192,193]. The contributions of band-edge and band-gap luminescence to the overall ECL are likely to be a function of the density of surfaces states, and their energetic depth. The quality of the core nanocrystal and its passivation (e.g. inorganic shell or ligand coating) are clearly important, but not necessarily the only considerations. Further study is needed to assess what role (if any) coreactants play in the creation of surface states. The influence of the local environment on ECL may also be important, particularly when QDs are immobilized at electrodes.

The ECL intensity observed in an experiment is a function of electron transfer rate, and therefore may also be a function of QD size. Jiang and Ju observed that the cathodic ECL intensity from CdSe QDs in the size range from 1.5 to 3.5 nm increased sharply to a maximum at 2.5 nm before decreasing as the size further increased [193]. The rise in ECL intensity was attributed to the decrease in the energy of the QD CB with increasing size, and a concomitant decrease in the energy of surface states. The basis for the latter hypothesis was cyclic voltammetry experiments by Poznyak et al. that demonstrated a positive shift in the oxidation potential of surface states with increasing QD size [171]. The decline in ECL intensity was attributed to the decrease in surface area-to-volume ratio at larger QD sizes. Additional observations by Poznyak et al. further suggest the importance of QD size and surface states [192]. Strong band-edge cathodic ECL was observed with films of yellow and red emitting CdSe QDs. However, a combination of band-edge and band-gap ECL with weak intensity was observed with films of green emitting QDs. Another parameter that affects electron transfer rates is conductivity, and this is important when working with electrode-supported films of QDs. In one study, it was suggested that a difference in conductivity between CdSe and CdSe/ZnS QDs was the source of a 100-fold difference in ECL intensity between films of otherwise similar composition [192]. As described in Section 3.4.2, altering the composition of QD films can enhance conductivity and ECL intensity.

3.4.2. Applications

Several research groups have made contributions to the development of ECL biosensors based on QDs. Some of these examples completely satisfy our introductory definition of QDs as integrated components, while others somewhat stretch the definition due to the absence of QD bioconjugation. However, all the examples satisfy the criterion of being present in the sample throughout the

analysis. The interested reader can refer to the literature for examples of QDs as non-integrated ECL labels in bioanalysis [194,195]. In this section we introduce the notation $_x$QD, where x denotes the position of the first exciton peak at x nm in the QD absorption spectrum (cf. QD_w for the peak PL). The cited references are categorized in Table 1.

In one of the earliest investigations in this field, Ju's group cast a solution of CdSe QD_{574} onto the surface of a paraffin impregnated graphite electrode (PIGE). This system was used to detect hydrogen peroxide in deaerated solutions down to levels as low as 0.1 μM [196]. The ability of hydrogen peroxide to act as a cathodic ECL coreactant was the basis of transduction. It follows that the ability to detect hydrogen peroxide enabled the development of a glucose biosensor [197]. A mixture of glucose oxidase (GOX) and MAA-coated QDs were successively cast onto a PIGE. An interesting aspect of this method was that the CT resistance measured for the co-cast film of QDs and GOX was lower than for a film of QD-GOX bioconjugates. The fast electron transfer kinetics was important in achieving efficient ECL. Considering glucose transduction, the activity of GOX in the presence of glucose converts dissolved oxygen into hydrogen peroxide. Although both of these species were able to act as ECL coreactants, oxygen was much more efficient. ECL was observed at −1.1 V (vs. Ag/AgCl). In the presence of glucose, the conversion of dissolved oxygen to hydrogen peroxide caused a decrease in QD ECL intensity. The response was linear with increases in glucose concentration over the range of 25–3000 μM, and the detection limit was 4 μM.

The QD-PIGE system was extended to the selective detection of glutathione (GSH) and L-cysteine (L-Cys) via cathodic ECL using hydrogen peroxide as a coreactant [193]. Reduced MAA-coated CdSe QD_{570} species reacted with hydrogen peroxide to form hydroxide radicals. The hydroxide radical behaved analogously to the sulfate radical anion in Eqs. (9) and (10), and its role as an intermediate was confirmed by EPR spectroscopy. ECL was observed at −1.1 V (vs. Ag/AgCl) and corresponded to band-edge PL. In biological molecules, thiols are particularly good scavengers of the hydroxide radical, being oxidized to the corresponding disulfide. It was therefore possible to detect GSH or L-Cys through a decrease in the observed ELC intensity. Although good selectivity was observed against other amino acids, any species that can scavenge the hydroxide radical is a potential interferent. The LODs for GSH and L-Cys were ca. 1–2 μM and a linear decrease in ECL intensity was observed up to ca. 50–60 μM. It is interesting to note that the MAA coating on the QD did not appear to interfere with the reaction between the QDs and the hydroxide radical. This was attributed to the different reactivity of thiolate groups that coordinated with the QD surface (RS^-QD), as compared to thiols in bulk solution (RSH). Wang and coworkers developed a second QD-ECL method for the detection of GSH, but with selectivity against L-Cys [198]. The addition of graphene oxide to the ECL sample solution was used to obtain this selectivity, and also to avoid potentially harsh oxidants that are typically used as coreactants. The graphene oxide enhanced the ECL intensity approximately five-fold by facilitating both the production superoxide anion from dissolved oxygen, and also the formation of hole-injected MAA-coated CdTe $_{543}$QD at anodic potential. Maximum ECL intensity was observed using 1.2 μg mL^{-1} of graphene at pH 9.5. The presence of GSH in a sample decreased the ECL intensity linearly in the range of 40–430 ng mL^{-1}. The selectivity for GSH over L-Cys was attributed to differences in affinity for the graphene oxide, and the method was used to measure GSH in a pharmaceutical drug sample.

In addition to graphene oxide, carbon nanotubes (CNTs) have been used to enhance the cathodic ECL intensity observed with QDs. The enhancement is attributed to a reduced barrier for electron injection, resulting in a lower onset potential and increased ECL intensity [199]. This enhancement is important since QDs are typically poorer ECL emitters than the more commonly used ruthenium complexes or luminol. Wang et al. have developed a biosensor for acetylcholine and choline using a PIGE incorporating multi-walled CNT-QD conjugates [200]. The CdS $_{480}$QD were synthesized on the CNTs *in situ* and the QD-CNT conjugates were found to provide a five-fold enhancement in ECL intensity compared to QDs alone. The enzymes acetylcholine esterase and choline oxidase were immobilized on the QD-CNT-modified PIGE. A byproduct of the catalytic cycles of these enzymes was hydrogen peroxide—a coreactant for cathodic QD ECL. Increasing sample concentrations of acetylcholine or choline increased the observed ECL approximately linearly, with LODs of 0.8 and 1.7 μM, respectively. The transduction mechanism is illustrated in Fig. 8b. The ECL onset and peak potentials were at −0.58 and −1.02 V (vs. Ag/AgCl) —approximately 0.40 and 0.28 V less negative, respectively, than without CNTs. The shift to more positive potentials reduced the possibility of electrochemical interference, and decreased the cathodic decomposition of hydrogen peroxide (which prevents its ECL reaction). In contrast to the glucose sensor developed by Jiang and Ju [197], this method was insensitive to dissolved oxygen. As a consequence, the production of hydrogen peroxide allowed signal-on detection.

CNTs have also been used to enhance QD ECL in the development of immunosensors. For example, Jie et al. prepared a gold electrode with a composite film of chitosan modified multi-walled CNTs, CdSe $_{496}$QD, and 3-aminopropyltriethoxysilane (APTES) [201]. In this case, the CNTs enhanced the ECL intensity by 2.5-fold, and the APTES enhanced the ECL a further 20-fold for an overall 50-fold enhancement. The enhancement was attributed to a catalytic effect of the APTES towards the reduction of the coreactant, peroxydisulfate. A biorecognition layer was formed by the immobilization of anti-human IgG, and exposure to bovine serum albumin (BSA) to block adsorption sites. The addition of the proteins increased the CT resistance, thereby reducing the ECL intensity. The formation of immunocomplexes further increased the CT resistance, and a linear decrease in ECL intensity (at −1.37 V vs. Ag/AgCl) was observed with increasing target IgG concentration. The LOD was 1 pg mL^{-1} and the biosensor was validated against an enzyme linked immunosorbent assay (ELISA). Jie et al. constructed a similar immunoassay using a layer-by-layer approach [202]. Multi-walled CNTs were coated with PDDA, MAA-coated CdSe $_{480}$QD, a second PDDA layer, and gold nanoparticles (Au NPs), before final modification with anti-human IgG. The CNTs increased the cathodic ECL intensity three-fold using peroxydisulfate as a coreactant. Detection was again based on the decrease in ECL intensity due to the formation of immunocomplexes. The LOD was 0.6 pg mL^{-1}. Fig. 8c illustrates the general transduction mechanism for ECL immunosensors that rely on changes in CT resistance.

The incorporation of Au NPs into QD-ECL biosensor design has the effect of increasing ECL intensity. For example, Jie et al. reported an increase of ca. 1.7 orders of magnitude in CdSe $_{451}$QD ECL intensity by incorporating a layer of Au NPs on an electrode [203]. The enhancement was attributed to a decreased CT resistance resulting from the increased surface area and conductivity imparted by the Au NPs. This system was used to develop a cathodic ECL immunoassay for human prealbumin with a 10 pg mL^{-1} LOD [203]. A similar design was used to develop a CdS $_{374}$QD-ECL immunoassay for low-density lipoprotein with a 6 pg mL^{-1} LOD [204]. In both cases, an electrode was modified with successive layers of Au NPs, QDs, and antibodies. The decrease in ECL intensity caused by immunocomplex formation was the basis for detection.

Many of the QD-ECL biosensors described in this section were robust and had good reproducibility. Relative standard deviations between analyses with a single electrode were ca. 1–10%, and ≤10% between different electrode preparations [193,196,197,200–204]. Many of the sensors were stored for 30 days or more without significant loss of function [193,196,197,201,202]. QD-ECL immunoassays

were also regenerated by glycine-HCl buffer at pH 2.8 with relative standard deviations of ≤10% between cycles of use [201–203].

In contrast to the above examples of immunoassays, Shan et al. used Au NPs to switch between low and high intensity ECL as a function of target nucleic acid hybridization [205]. Manganese doped CdS QDs were coated onto a glassy carbon cathode and modified with Au NP conjugated hairpin nucleic acid probes. Peroxydisulfate was used as the coreactant. With the hairpin in the closed conformation, the ECL (at −1.3 V vs. standard calomel electrode, SCE) was quenched by 25%. Upon target hybridization and opening of the hairpin, an ECL enhancement of 55% was observed. The switching was based on the ability of Au NPs to quench or enhance luminescence as a function of proximity. Target nucleic acid could be detected at concentrations as low as 50 aM with discrimination of single nucleotide polymorphisms (SNPs). An interesting aspect of this work was that the manganese doping appeared to increase the stability of reduced QDs.

Ju's research team has also developed bioprobes utilizing anodic QD ECL. In one study, a method was developed for the detection of dopamine using MAA-coated CdSe $_{424}$QD and sulfite as a coreactant [206]. QDs and sulfite were oxidized at the anode to hole-injected QDs and sulfite radical anions, respectively. The sulfite radical further reacted with dissolved oxygen to form the superoxide anion. The superoxide anion injected an electron into a QD, and excited state QDs were produced via the reaction in Eq. (6). Although the sulfite was not strictly necessary, it increased the ECL intensity (at +0.93 V vs. Ag/AgCl) by greater than fourteen-fold. The addition of dopamine quenched the observed ECL with a Stern–Volmer concentration dependence. The dynamic range for dopamine response was 0.5–70 μM. The dopamine did not directly act as a quencher. Rather, its oxidized product, an *o*-benzoquinone, was formed at the anodic potential and quenched the excited state of QDs via collisional energy transfer [180]. The quenching observed in the presence of dopamine was approximately sixteen-fold and seven-fold stronger than for the common interferents ascorbic acid and uric acid, respectively. A second study used MPA-coated CdTe QD$_{590}$ with sulfite as an anodic ECL co-reactant to detect tyrosine [207]. The ECL originated from the band-edge. Analogous to the dopamine method, the oxidized *o*-quinone product of tyrosine efficiently quenched ECL (at +0.90 V vs. Ag/AgCl). Although anodic oxidation of the tyrosine was possible, the addition of tyrosinase increased the rate of oxidation, and resulted in stronger quenching. Without tyrosinase, the LOD was 46 nM; with tyrosinase the LOD decreased to 0.1 pM. Potential interferents such as uric acid, ascorbic acid, L-phenylalanine, and L-tryptophan could be tolerated at concentrations 1000 20,000-fold higher than tyrosine. However, as expected, dopamine and other compounds that yielded quinone oxidation products interfered with analyses.

To the best of our knowledge, multiplexed biosensing using QD-ECL has not been developed. Arrays of individually fabricated electrodes represent one potential approach to multiplexing, and are well suited for affinity sensing. The modulation of ECL intensity by changes in CT resistance allows a single coreactant to be used across an electrode array in a single solution. However, other strategies may require separate reaction compartments (e.g. on-chip) due to the potential for cross-reactivity with coreactants. Another approach to multiplexing is to encode information about target binding as a function of QD emission wavelength (i.e. colour). In principle, this could allow multiplexing using a single electrode. However, the current literature suggests several challenges in this respect—particularly the quality of QD ECL emission. Although ECL originating from the band-edge has been obtained and used in sensing [207], there are many examples where ECL originating from the band-gap (i.e. surface states) [199,205,206], or a mixture of band-edge and band-gap emission [193], has also been used for sensing. Band-gap emission is not useful for multiplexing since it is broad and not readily size-tunable. Furthermore, the QDs used in ECL experiments have been largely synthesized via aqueous methods. In contrast to QDs synthesized in hot coordinating solvent (e.g. [26,27]), these QDs tend to have very broad emission. Typical FWHM are often > 70 nm and thus not well suited for multiplexing. Although there is clearly significant potential for biosensors using ECL for transduction, more development is needed to maximize the impact of QDs in this field.

4. Solid-phase assays

4.1. Immobilization of QDs

The immobilization of QDs for interfacial assays has several advantages over homogeneous solution phase assays. Bioconjugates can be prepared without time-consuming purification methods such as electrophoresis, size-exclusion columns, or dialysis—washing of the solid interface can be sufficient to remove excess biomaterials. Immobilization may also provide more flexibility with QD surface chemistry. In contrast to QDs in bulk solution, QDs immobilized at an interface have less strict requirements for colloidal stabilization and solubility. Therefore, there is potentially greater versatility in the selection of coatings, coupling chemistries, and solvent systems that can be used for the assembly of QD-based biosensors and bioprobes. QD immobilization may also provide advantages for detection. Real samples can be complex biological matrices. After target binding in the complex matrix, removal of the solid substrate and subsequent washing may eliminate undesirable background associated with sample autofluorescence or scattering that is largely unavoidable in solution phase assays. While both solution-phase and immobilized QDs can be optically interrogated by linear and non-linear far-field techniques, immobilized QDs can also be interrogated by near-field techniques including evanescent waves [208–211] and whispering gallery modes [212], surface plasmon enhanced fluorescence [213], enhanced fluorescence from structured metal surfaces [214,215], and photonic crystal enhanced fluorescence [216]. Although these techniques are also suitable for solid-phase assays using QDs as non-integrated labels, the direct immobilization of QD-bioconjugates at a solid interface potentiates reusability—an essential feature of a true QD-based biosensor.

The immobilization of QDs for assay and biosensor development is not trivial, and the criteria for a successful immobilization strategy depend on the type of analysis. Physical entrapment, covalent attachment, coordination/dative bonds, electrostatic attraction, other affinity interactions, or combinations thereof, can provide the basis for QD immobilization. Selected examples from the literature include: hetero-bifunctional coordinating ligands that interact with both the QD and the solid surface [217]; covalent coupling between surface-bound functional groups and the QD coating [218–221]; the biotin–Avidin interaction [222,223]; casting Langmuir–Blodgett films [224]; fabrication of layer-by-layer assemblies [225]; incorporation into sol–gels [226], hydro-gels [227], or micro-gels [228]; and biomolecular tethers [229]. Additional examples are described and cited later in this section as examples of solid-phase assays. The selected immobilization method must address criteria such as the available means of bioconjugation, the required proximity between QDs and affinity probes (e.g. FRET), and the size and mobility of the target analyte. In some applications, the degree of QD loading at the interface and the stability of the immobilization may also be important. Moreover, the ECL immunosensors in Section 3.3.2 are an example where CT resistance is important, and the proximity between QDs and bioaffinity probe is less so. In general, most solid-phase bioassay and biosensor assemblies for larger targets (e.g. nucleic acids, proteins) will require the immobilization of QDs as thin films on a

substrate, rather than embedded in a three-dimensional matrix. Inspired by the success of bidentate thiolates as ligands for colloidal QDs [43], our group developed multidentate surface ligand exchange for the immobilization of QDs as thin films [210,230]. Using solid-phase synthesis, fused silica substrates were modified with an aminosilane, which was further modified to yield a high density of surface tethers with two pendant bidentate thiols. Several of these surface ligands were capable of coordinating to the surface of CdSe/ZnS QDs for interfacial immobilization as thin film. The upper surfaces of the QDs were accessible for further bioconjugation, providing the basis for the development of solid-phase hybridization assays.

4.2. Applications

One of the earliest examples of the immobilization of QDs for FRET-based assay development was by Tran et al. [231]. Negatively charged DHLA-coated QDs were immobilized on poly-L-lysine coated glass slides using electrostatic assembly. Dark quencher-labeled antibodies were immobilized on the QDs as a second layer assembled through electrostatic attraction via a dimeric bifunctional protein G-basic zipper molecular adapter with high affinity for the F_c region of IgG. The immobilized QD PL decreased with increasing immobilization of the quencher labeled IgG. However, this work did not go beyond a model for the surface assembly of QD bioconjugates, and a complete immunoassay was not developed.

Two other early studies examined the immobilization of the QD-MBP conjugates for the detection of maltose. In one study, $QD_{555/570}$ were modified with both MBP and avidin. The latter allowed attachment to a NeutrAvidin coated surface by either a biotinylated MBP bridge or an IgG bridge [232]. In a second study, DHLA-coated $QD_{510/530/590}$ were immobilized via a rigid designer peptide [95]. The peptide C-terminus was modified with a hexahistidine sequence to coordinate the QD surface; the N-terminus was biotinylated for attachment to a NeutrAvidin coated substrate. The immobilized QDs were further modified with pentahistidine appended MBP, demonstrating the solid-phase derivatization of QDs. To generate an analytical signal, the MBP was labeled at an allosterically sensitive site with a Cy3 acceptor. The conformational change associated with maltose binding quenched the FRET-sensitized Cy3 PL. An important conclusion of this study was that both the LOD and dynamic range of the immobilized construct were less favourable than the solution phase analog. The change in local environment and loss of degrees of freedom caused by surface immobilization are not trivial, and this study highlights that the immobilization strategy can be as significant as the transduction strategy.

Our group has developed a non-traditional approach to FRET-based assays that utilizes mixed films of immobilized QDs and oligonucleotide probes for nucleic acid detection. In contrast to the centrosymmetric colloidal donor–acceptor(s) model (Fig. 2a), the mixed film architecture we have investigated is a two-dimensional interfacial array of QD donors with which acceptors can be associated via nucleic acid hybridization. There are two important differences between these architectures: (1) donor–acceptor stoichiometry; and (2) donor–acceptor distance. In the immobilized film (Fig. 2c), multiple donors can interact with multiple acceptors over a distribution of donor–acceptor distances. The number of potential energy transfer pathways (including the possibility of donor–donor interactions) and corresponding efficiencies are clearly different between the two systems. The ability of an acceptor to potentially interact with multiple donors is unique to the interfacial immobilization of QDs. In our laboratory, we have explored the development of solid-phase hybridization assays on this basis [208–211]. Multidentate surface ligand exchange [230] was used for the preparation of films of QDs, and transduction was based on hybridization mediated FRET between QD donors and fluorescent acceptors, similar to our earlier work described in Section 3.1.2 [123].

The selective interfacial detection of nucleic acids using QDs and FRET was first demonstrated via the immobilization MPA-coated QD_{538} on optical fibers [208]. The immobilized QDs were modified with thiol terminated oligonucleotide probes, and the remaining surface coated with denatured BSA. The denatured BSA was essential for blocking non-specific adsorption and achieving selectivity. Interfacial hybridization provided the proximity for FRET and allowed the detection of target oligonucleotides at concentrations as low as 5 nM. Regeneration and reuse was possible over seven cycles, although both the signal level and the degree of regeneration decreased with each cycle. Working above room temperature enhanced the selectivity of the assay. At 40 °C, a contrast of ca. 10:3 was obtained between fully complementary and three base-pair mismatched target sequences (c.f. 1.0:1.4 at room temperature). However, SNP discrimination was not achieved. An improvement in analytical performance was possible by modifying the interfacial chemistry used in the QD-FRET hybridization assay [209]. The immobilized MPA-QDs were coated with a layer of Neutravidin and biotinylated oligonucleotide probes. Secondary exposure to BSA was used to block any remaining adsorption sites. The detection of a single target was possible using immobilized QD_{530} with a Cy3 acceptor, or QD_{622} with an A647 acceptor. Compared to the previous study, larger FRET signals were obtained, enabling detection limits as low as 1 nM. The assay retained signal and selectivity in serum, and against a large background of non-complementary genomic DNA. Assay times varied from 1 to 3 h, and the modified fibers could be stored for at least a week. It was possible to avoid target labeling by introducing a sandwich assay with an acceptor dye-labeled reporter oligonucleotide, and without a significant increase in LOD. SNP discrimination was possible in either format, with contrast as high as 31:1, by incorporating formamide into samples at room temperature. In comparison to the previous study, this assay offered less potential for regeneration and reuse. Additional study has identified that the limited stability of the protein layer was largely responsible for the incomplete regeneration that was observed. An improvement was possible by cross-linking the protein layer, although still insufficient for multiple cycles of use without any loss of performance [233]. Despite this limitation, the interfacial chemistry in this assay was otherwise ideal for exploring the development of multiplexed assays based on QDs and FRET.

A two-plex hybridization assay was possible through the co-immobilization of QD_{530} and QD_{622}, and the co-immobilization of two different oligonucleotide probe sequences, as mixed films on optical fibers [209]. The mixed film approach potentiated the facile preparation of the assay. Two detection channels were created using Cy3 and A647 acceptors, where probe-target hybridization provided the proximity for FRET. The ratio of dye acceptor-to-QD donor PL was proportional to the target concentration in each channel, where the individual contributions of each QD and dye to the overall PL were extracted via deconvolution. The estimated LODs were 3 and 1 nM in the Cy3 and A647 channels, respectively. The assay format is illustrated in Fig. 9a. SNP discrimination was also possible in the two-plex format via the addition of formamide. Moreover, it was possible to tune the response in each detection channel via changes in the ratio of the corresponding immobilized probes (i.e. probe dilution).

A second two-plex assay was developed using a single colour of immobilized QDs [210]. QD_{528} were combined with Cy3 and RhR as acceptor dyes. Both dyes had spectral overlap with the QD donor, and it was possible to deconvolute their emission spectra in order to obtain two detection channels. The assay LOD was 10 nM. From a materials perspective, the advantage of this strategy was that selective two-plex detection was possible using only

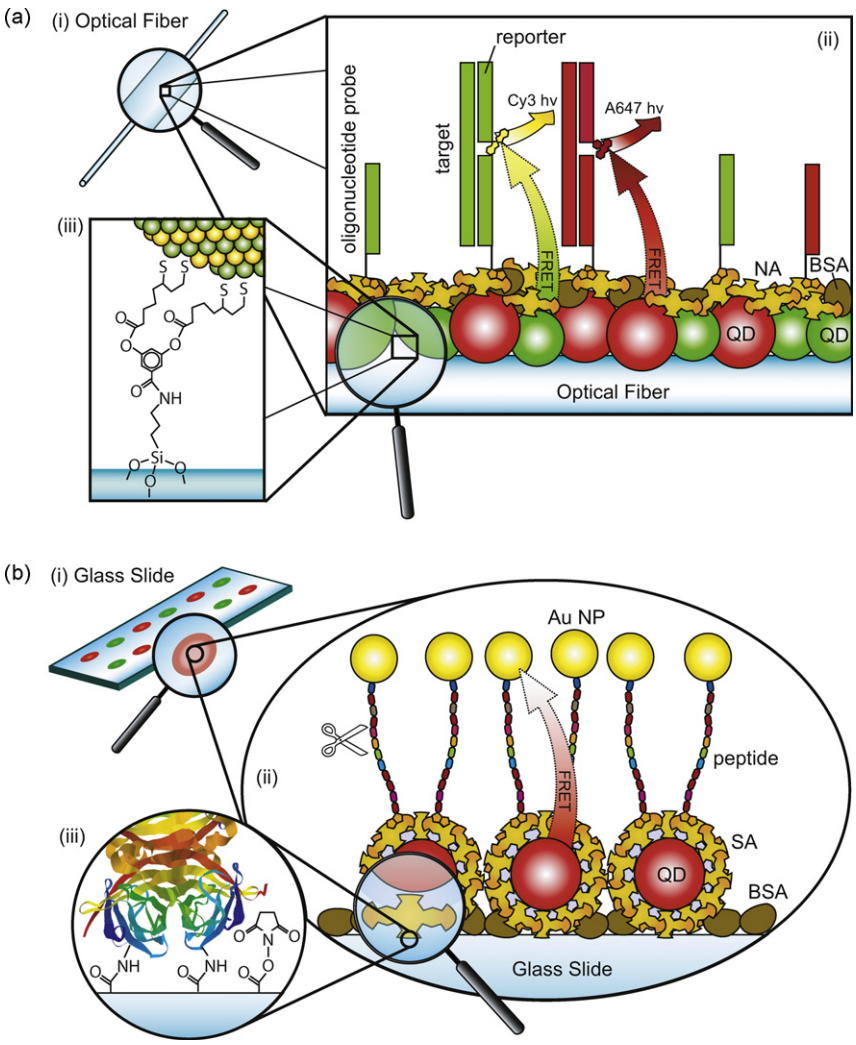

Fig. 9. Solid-phase FRET assays incorporating immobilized QDs. (a) a multiplexed nucleic acid hybridization assay [209–211,234] depicted at three size-scales: (i) fused silica optical fiber substrate; (ii) interfacial QD-bioconjugates; (iii) and QD immobilization via multidentate surface ligand exchange. In (ii), energy transfer from QDs to acceptor dye-labeled reporter oligonucleotides in a sandwich format allows selective detection. The acceptor emission is the analytical signal. (b) A multiplexed protease assay [141] depicted at three size-scales: (i) glass slide substrate; (ii) interfacial QD-bioconjugates; and (iii) QD immobilization via amide bond formation between a Streptavidin coating and a succinimide ester activated surface. In (ii), the QDs are efficiently quenched by Au NP-peptide conjugates. Protease activity (scissors) cleaves the peptide, thereby restoring PL and providing an analytical signal. The two colours of spots on the substrate in (i) illustrate the multiplexing capability. Further details on the solid-phase assays in (a) and (b) can be found in the main text. Figures not to scale.

one type of QD donor. From the analytical perspective, the spectral bandwidth was ca. 125 nm, compared to 250 nm with the previous two-QD-donor strategy. Furthermore, the study also helped elucidate important aspects of multiplexed hybridization assays based on mixed films of QDs and oligonucleotide probes. For example, the time to reach equilibrium response was approximately independent of probe dilution, and multiplexing therefore did not require longer hybridization times. It was also possible to clarify the origin of decreases in FRET-signal when moving from one-plex to two-plex assays, or when the relative amount of one probe decreased in a two-plex assay. The former was initially attributed to the combination of probe dilution and QD dilution. QD dilution refers to the relative quantities of QD_{530} and QD_{622}, which was expected to alter the average donor–acceptor distance for each FRET-pair in a mixed film [209]. Linear changes in FRET-signal were observed with changes in probe ratio in two-plex assays with one [210] and two QD donors [209]. This suggested that the average donor–acceptor distance in mixed films with two immobilized QDs was not significantly altered by changes in the probe ratio. Thus, acceptor number density appeared to be the driving force for signal changes as a function of probe ratio, and when moving from a one-plex to two-plex assay (although the QD_{530}-to-QD_{622} ratio may also be important [211]). Therefore, a potential route to signal enhancement in future assays designs is the association of multiple acceptor dyes with a single hybridization event. We have recently found that signal enhancements of >70% and >40% were obtained in one-plex and two-plex sandwich assays, respectively, that utilized reporter oligonucleotides labeled at both termini with an A647 acceptor dye (cf. one terminus) [234].

The multiplexing potential of QD-FRET methods is limited when compared to that of QD-based optical barcodes. Nonetheless, as described previously, the combination of immobilized QDs and their use as donors in FRET provides a unique set of advantages. The development of higher order multiplexing strategies that retain these advantages is important to their success in real applications. In our laboratory, we have also explored the development of three-plex and four-plex hybridization assays without the need for more than two colours of immobilized QD, and without sacrificing the advantages of a solid-phase two-plex assay [211,234]. The addition of another detection channel via the co-immobilization of a third QD donor was not necessarily the best approach. Moving to shorter or longer wavelengths would have required new QD

materials (e.g. CdS, CdTe), may have created challenges with both wavelength-dependent photodetector efficiency or excitation efficiency, and caused greater QD dilution. Instead, a third detection channel was incorporated in sandwich assays by using the direct excitation of reporter oligonucleotides labeled with Pacific Blue (PB) [211]. Efficient excitation of both the PB and QDs was possible, and the PB emission was readily resolved with only moderate expansion of the region of the visible spectrum used in the analysis. Two formats were possible for selective three-plex detection: the combination of PB, Cy3, and A647, with both QD_{528} and QD_{618} donors; or alternatively, the combination of PB, Cy3, and RhR, with only a QD_{528} donor. Probe stoichiometry was used to balance the FRET signals in each detection channel, compensating for differences in direct excitation efficiency (PB) and FRET efficiency (Cy3, RhR, A647). SNP discrimination was possible in three-plex format; however, optimization of probe lengths was required to ensure that the SNP hybridization could be suppressed in one channel without suppressing complement hybridization in the other channels. A third approach to a three-plex hybridization was also explored and did not incorporate PB [234]. Immobilized QD_{528} and QD_{618} donors were combined with Cy3, RhR, and A647 to comprise a two donor-three acceptor FRET strategy. Analytically, three-plex assays relying on a PB-channel are better suited to detecting lower concentrations of target. This is due to the potential uncertainty in the deconvolution of the overlapping emission spectra of the Cy3, RhR, and QD_{618} in the two donor–three acceptor strategy. Nonetheless, the advantage of this strategy was that the addition of a PB channel potentiated a four-plex hybridization assay [234]. Although proof-of-concept was demonstrated, low FRET signals resulted from the high level of probe dilution in a mixed film of four different probe oligonucleotides and two QD donors. The loss of sensitivity was a hindrance to practical application, and highlights the need for the enhancement of FRET signals. If this can be satisfactorily achieved, four-plex assays that take advantage of both the immobilization of QDs, and their use as donors in multiplexed FRET, will become viable.

It should be noted that Zhang and Hu have also adopted the combination of the direct excitation of fluorescence and FRET using QDs for multiplexed nucleic acid detection [235]. Alexa Fluor 488 (direct excitation), Cy5 (acceptor), and QD_{605} (donor) were used in a homogeneous (i.e. solution phase) two-plex hybridization assay. The QDs were modified with two different oligonucleotide probes, and a sandwich assay format was used to associate the dyes with the QD via hybridization. Microcapillary flow and coincidence detection at the single molecule level were used for analysis.

In addition to our work, Feng et al. have also used the co-immobilization of multiple colours of QD to develop a solid-phase hybridization assay [236]. However, in this case, the multiple colours of QD were not used for multiplexing. Instead, the layer-by-layer assembly of QD_{561}, QD_{594}, and QD_{614} inside a porous anodic aluminum oxide template was used to create an energy transfer relay. The excitation of the outer layer of QD_{561} transferred along the band-gap gradient to the inner layer of QD_{614}. This inner layer was functionalized with oligonucleotide probes, and hybridization with Cy5-labeled target sequences added an additional step in the transfer. The FRET-sensitized Cy5 PL provided an analytical signal with a sub-nanomolar LOD. Although not fully developed into an assay, Qi et al. devised a transduction strategy that used both FRET and photovoltaic responses to detect nucleic acid hybridization [237]. Carboxyl-coated QDs were covalently coupled to an APTES film between two electrodes on a silicon dioxide substrate. The immobilized QD_{590} were cross-linked with double-stranded DNA that incorporated a Cy5 label. This generated two analytical signals: FRET-sensitized Cy5 PL and a significant photocurrent between the two electrodes. An increase in the photocurrent was characteristic of fully complementary duplex, and no significant photocurrent was observed for mismatched duplex. The study highlights the advantage of multimodal detection in potentially identifying false positive signals from non-specific adsorption, or discriminating between target and mismatched sequences without the need for thermal or chemical destabilization.

Solid-phase QD-FRET assays for protease activity have also been developed. Kim et al. immobilized spots of SA-coated QDs on a *N*-hydroxysuccinimide activated hydrogel glass slide [141]. BSA was used to block the remainder of surface. The subsequent immobilization of biotinylated peptides that were labeled with Au NPs resulted in $\geq$80% quenching of the QD PL. Specific cleavage of the peptide sequence by target protease activity restored the QD PL by release of the Au NP. This assay format is illustrated in Fig. 9b. Three-plex detection was possible by immobilizing three sets of spots corresponding to QD_{525}, QD_{605}, and QD_{655}. Each colour of QD was conjugated to a different peptide sequence specific to either MMP-7, caspase-3, or thrombin, respectively. The corresponding LODs were 10 ng mL^{-1}, 1 U mL^{-1}, and 20 ng mL^{-1}, respectively. The fabrication of all three QD-peptide conjugates via the biotin–SA interaction and the use of a common quencher for all three channels necessitated spatial registration (i.e. spots). However, the use of different QD emitters potentiates analysis via a simple PL spectrum without imaging to resolve the spatial registration. The same research group developed a similar one-plex assay for MMP-7 activity [142]. SA-coated QD_{525} were immobilized and conjugated with biotinylated peptides that were labeled with TAMRA as an acceptor. The analytical parameter was the ratio of QD-to-TAMRA PL, and increased with proteolytic activity. The LOD was 100 ng mL^{-1}. The lower LOD with Au NP-labeled peptide was likely due to the superior quenching efficiency of Au NPs. In both studies, the dynamic ranges were approximately three orders of magnitude, and analysis times were 1–2 h.

5. Summary and conclusions

This review has provided an extensive overview of the use of QDs as integrated components of assays, bioprobes, and biosensors. Integrated QDs serve as a scaffold for both bioconjugation and biorecognition, and are present in a system throughout a bioanalysis. In contrast to the use of QDs as simple labels, where unbound QDs are washed away to eliminate signal, the use of integrated QDs requires modulation of the QD luminescence in response to biorecognition events. Mechanisms such as FRET, BRET, and CT quenching have been used in this respect. Their strong distance dependence provides the basis for the transduction of biorecognition events that are associative (e.g. hybridization), dissociative (e.g. proteases), or result in conformation changes (e.g. ligand–receptor interactions). While the processes of FRET and BRET with QDs are generally well understood, many aspects of the CT quenching of QDs require further study. ECL has also been used with integrated QDs for assay and biosensor development. In this case, transduction is most commonly based on either changes in coreactant concentration due to enzyme activity, or changes in CT resistance due to binding events at a QD-modified electrode. However, due to the propensity towards band-gap emission in ECL methods, the impact of QDs has not yet been maximized in this area.

The coatings and the bioconjugation strategies used with QDs are a critically important consideration in the development of bioanalyses. Both compact ligand-based QD coatings and thicker polymeric QD coatings have been compatible with FRET and BRET as transduction methods. Compared to CT quenching or ECL, FRET and BRET have the smallest distance dependence and sensitivity to QD coating due to their through-space dipole–dipole interaction. In contrast, CT and ECL require electron transfer through short-range

orbital overlap. To date, only ligand-based QD coatings have been used with these methods of transduction. Furthermore, QD surface states have been identified as playing a role in CT quenching and ECL. Although this role is not yet fully characterized, QD coatings are expected to have influence. The QD bioconjugation method is important because it can potentially dictate the orientation and conformational mobility of conjugated biomolecules, the valence of QD-bioconjugates, and add thickness to the overall QD coating—all of which can influence the efficiency of FRET, BRET, and CT.

The development of bioanalyses that integrate QDs with FRET, BRET, CT quenching, and ECL-based transduction continues to grow. Currently, FRET-based methods are the most developed, and a large variety of both homogeneous solution-phase assays, and heterogeneous solid-phase assays, have been reported in the literature. Although the majority of work on the former has been *in vitro*, both FRET-based and CT-based bioprobes have been applied *ex vivo*. The continued development of *ex* vivo and *in vivo* bioanalyses will be a major thrust in this area of research over the next several years.

Acknowledgements

The authors are grateful to the Natural Sciences and Engineering Research Council of Canada (NSERC) for funding their research program. WRA is also grateful to the University of Toronto and the Ontario Ministry of Education and Training for a graduate fellowship (OGSST).

References

[1] C.B. Murray, C.R. Kagan, M.G. Bawendi, Annu. Rev. Mater. Sci. 30 (2000) 545–610.
[2] M. Bruchez, M. Moronne, P. Gin, S. Weiss, A.P. Alivisatos, Science 281 (1998) 2013–2016.
[3] W.C.W. Chan, S. Nie, Science 281 (1998) 2016–2018.
[4] I.L. Medintz, H.T. Uyeda, E.R. Goldman, H. Mattoussi, Nat. Mater. 4 (2005) 435–446.
[5] X. Michalet, F.F. Pinaud, L.A. Bentolila, J.M. Tsay, S. Doose, J.J. Li, G. Sundaresan, A.M. Wu, S.S. Gambhir, S. Weiss, Science 307 (2005) 538–544.
[6] A.M. Smith, H.W. Duan, A.M. Mohs, S. Nie, Adv. Drug Deliv. Rev. 60 (2008) 1226–1240.
[7] J. Rao, A. Dragulescu-Andrasi, H. Yao, Curr. Opin. Biotechnol. 18 (2007) 17–25.
[8] J.B. Delehanty, H. Mattoussi, I.L. Medintz, Anal. Bioanal. Chem. 393 (2009) 1091–1105.
[9] W.R. Algar, M. Massey, U.J. Krull, Trends Anal. Chem. 28 (2009) 292–306.
[10] I.L. Medintz, H. Mattoussi, Phys. Chem. Chem. Phys. 11 (2009) 17–45.
[11] R. Gill, M. Zayats, I. Willner, Angew. Chem. Int. Ed. 47 (2008) 7602–7625.
[12] W.R. Algar, U.J. Krull, Anal. Bioanal. Chem. 391 (2008) 1609–1618.
[13] D. Geho, N. Lahar, P. Gurnani, M. Huebschman, P. Herrmann, V. Espina, A. Shi, J. Wulfkuhle, H. Garner, E. Petricoin, L.A. Liotta, K.P. Rosenblatt, Bioconjug. Chem. 16 (2005) 559–566.
[14] D. Gerion, F.Q. Chen, B. Kannan, A.H. Fu, W.J. Parak, D.J. Chen, A. Majumdar, A.P. Alivisatos, Anal. Chem. 75 (2003) 4766–4772.
[15] J.H. Kim, K.S. Seo, J. Wang, IEEE Sens. J. 6 (2006) 248–253.
[16] A.P. Alivisatos, J. Phys. Chem. 100 (1996) 13226–13239.
[17] A.M. Smith, S. Nie, Acc. Chem. Res. 43 (2010) 190–200.
[18] O.I. Micic, C.J. Curtis, K.M. Jones, J.R. Sprague, A.J. Nozik, J. Phys. Chem. 98 (1994) 4966–4969.
[19] D. Battaglia, X.G. Peng, Nano. Lett. 2 (2002) 1027–1030.
[20] R.G. Xie, X.G. Peng, J. Am. Chem. Soc. 131 (2009) 10645–10651.
[21] Y.W. Cao, U. Banin, J. Am. Chem. Soc. 122 (2000) 9692–9702.
[22] T. Pons, N. Lequeux, B. Mahler, S. Sasnouski, A. Fragola, B. Dubertret, Chem. Mater. 21 (2009) 1418–1424.
[23] W. Jiang, A. Singhal, J.N. Zheng, C. Wang, W.C.W. Chan, Chem. Mater. 20 (2006) 4845–4854.
[24] J.H. Warner, A. Hoshino, K. Yamamoto, R.D. Tilley, Angew. Chem. Int. Ed. 44 (2005) 4550–4554.
[25] D.S. English, L.E. Pell, Z.H. Yu, P.F. Barbara, B.A. Korgel, Nano Lett. 2 (2002) 681–685.
[26] M.A. Hines, P. Guyot-Sionnest, J. Phys. Chem. 100 (1996) 468–471.
[27] Z.A. Peng, X.G. Peng, J. Am. Chem. Soc. 123 (2001) 183–184.
[28] L. Qu, Z.A. Peng, X. Peng, Nano Lett. 1 (2001) 333–337.
[29] B.O. Dabbousi, J. Rodriguez-Viejo, F.V. Mikulec, J.R. Heine, H. Mattoussi, R. Ober, K.F. Jensen, M.G. Bawendi, J. Phys. Chem. B 101 (1997) 9463–9475.
[30] X. Peng, M.C. Schlamp, A.V. Kadavanich, A.P. Alivisatos, J. Am. Chem. Soc. 119 (1997) 7019–7029.
[31] C.B. Murray, D.J. Norris, M.G. Bawendi, J. Am. Chem. Soc. 115 (1993) 8706–8715.
[32] Y. Yin, A.P. Alivisatos, Nature 437 (2005) 664–670.
[33] A.L. Rogach, T. Franzl, T.A. Klar, J. Feldmann, N. Gaponik, V. Lesnyak, A. Shavel, A. Eychmueller, Y.P. Rakovich, J.F. Donegan, J. Phys. Chem. C 111 (2007) 14628–14637.
[34] J.J. Li, Y.A. Wang, W. Guo, J.C. Keay, T.D. Mishima, M.B. Johnson, X. Peng, J. Am. Chem. Soc. 123 (2001) 12567–12575.
[35] W.R. Algar, U.J. Krull, in: A. Merckoçi (Ed.), Biosensing Using Nanomaterials, John Wiley & Sons, Inc., Hoboken, 2009, pp. 199–245.
[36] S.F. Lee, M.A. Osborne, Chem. Phys. Chem. 10 (2009) 2174–2191.
[37] U. Resch-Genger, M. Grabolle, S. Cavaliere-Jaricot, R. Nitschke, T. Nann, Nat. Methods 5 (2008) 763–775.
[38] W.R. Algar, U.J. Krull, Chem. Phys. Chem. 8 (2007) 561–568.
[39] J. Aldana, N. Lavelle, Y. Wang, X. Peng, J. Am. Chem. Soc. 127 (2005) 2496–2504.
[40] V.V. Breus, C.D. Heyes, K. Tron, G.U. Nienhaus, ACS Nano 3 (2009) 2573–2580.
[41] W.H. Liu, H.S. Choi, J.P. Zimmer, E. Tanaka, J.V. Frangioni, M. Bawendi, J. Am. Chem. Soc. 129 (2007) 14530–14531.
[42] A. Dif, F. Boulmedais, M. Pinot, V. Roullier, M. Baudy-Floc'h, F.M. Coquelle, S. Clarke, P. Neveu, F. Vignaux, R. Le Borgne, M. Dahan, Z. Gueroui, V. Marchi-Artzner, J. Am. Chem. Soc. 131 (2009) 14738–14746.
[43] H.T. Uyeda, I.L. Medintz, J.K. Jaiswal, S.M. Simon, H. Mattoussi, J. Am. Chem. Soc. 127 (2005) 3870–3878.
[44] K. Susumu, H.T. Uyeda, I.L. Medintz, T. Pons, J.B. Delehanty, H. Mattoussi, J. Am. Chem. Soc. 129 (2007) 13987–13996.
[45] B.C. Mei, K. Susumu, I.L. Medintz, J.B. Delehanty, T.J. Mountziaris, H. Mattoussi, J. Mater. Chem. 18 (2008) 4949–4958.
[46] W. Liu, M. Howarth, A.B. Greytak, Y. Zheng, D.G. Nocera, A.Y. Ting, M.G. Bawendi, J. Am. Chem. Soc. 130 (2008) 1274–1284.
[47] F. Dubois, B. Mahler, B. Dubertret, E. Doris, C. Mioskowski, J. Am. Chem. Soc. 129 (2007) 482–483.
[48] J. Wang, J. Xu, M.D. Goodman, Y. Chen, M. Cai, J. Shinar, Z.Q. Lin, J. Mater. Chem. 18 (2008) 3270–3274.
[49] X. Gao, Y. Cui, R.M. Levenson, L.W.K. Chung, S. Nie, Nat. Biotechnol. 22 (2004) 969–976.
[50] T. Pellegrino, L. Manna, S. Kudera, T. Liedl, D. Koktysh, A.L. Rogach, S. Keller, J. Rädler, G. Natile, W.J. Parak, Nano Lett. 4 (2004) 703–707.
[51] W. Liu, A.B. Greytak, J. Lee, C.R. Wong, J. Park, L.F. Marshall, W. Jiang, P.N. Curtin, A.Y. Ting, D.G. Nocera, D. Fukumura, R.K. Jain, M.G. Bawendi, J. Am. Chem. Soc. 132 (2010) 472–483.
[52] A.M. Smith, H. Duan, M.N. Rhyner, G. Ruan, S. Nie, Phys. Chem. Chem. Phys. 8 (2006) 3895–3903.
[53] T. Pons, H.T. Uyeda, I.L. Medintz, H. Mattoussi, J. Phys. Chem. B 110 (2006) 20308–20316.
[54] P. Wu, Y. He, H.F. Wang, X.P. Yan, Anal. Chem. 82 (2010) 1427–1433.
[55] X. Ji, J. Zheng, J. Xu, V.K. Rastogi, T.C. Chen, J.J. DeFrank, R.M. Leblanc, J. Phys. Chem. B 109 (2005) 3793–3799.
[56] E.R. Goldman, I.L. Medintz, J.L. Whitley, A. Hayhurst, A.R. Clapp, H.T. Uyeda, J.R. Deschamps, M.E. Lassman, H. Mattoussi, J. Am. Chem. Soc. 127 (2005) 6744–6751.
[57] Q. Wei, M. Lee, X. Yu, E.K. Lee, G.H. Seong, J. Choo, Y.W. Cho, Anal. Biochem. 358 (2006) 31–37.
[58] S. Pathak, M.C. Davidson, G.A. Silva, Nano Lett. 7 (2007) 1839–1845.
[59] H. Mattoussi, J.M. Mauro, E.R. Goldman, G.P. Anderson, V.C. Sundar, F.V. Mikulec, M.G. Bawendi, J. Am. Chem. Soc. 122 (2000) 12142–12150.
[60] I.L. Medintz, A.R. Clapp, H. Mattoussi, E.R. Goldman, B. Fisher, J.M. Mauro, Nat. Mater. 2 (2003) 630–638.
[61] B. Tang, L. Cao, K. Xu, L. Zhuo, J. Ge, Q. Li, L. Yu, Chem. Eur. J. 14 (2008) 3637–3644.
[62] M. Ikanovic, W.E. Rudzinski, J.G. Bruno, A. Allman, M.P. Carrillo, S. Dwarakanath, S. Bhahdigadi, P. Rao, J.L. Kiel, C.J. Andrews, J. Fluoresc. 17 (2007) 193–199.
[63] D. Zhou, J.D. Piper, C. Abell, D. Klenerman, D.J. Kang, L. Ying, Chem. Commun. (2005) 4807–4809.
[64] J.H. Kim, D. Morikis, M. Ozkan, Sens. Actuators B 102 (2004) 315–319.
[65] C.Y. Zhang, H.C. Yeh, M.T. Kuroki, T.H. Wang, Nat. Mater. 4 (2005) 826–831.
[66] M. Levy, S.F. Cater, A.D. Ellington, Chem. Biol. Chem. 6 (2005) 2163–2166.
[67] M.M.C. Sun, K.S. Beam, C.G. Cerveny, K.J. Hamblett, R.S. Blackmore, M.Y. Torgov, F.G.M. Handley, W.C. Ihle, P.D. Senter, S.C. Alley, Bioconjug. Chem. 16 (2005) 1282–1290.
[68] B. Barat, S.J. Sirk, K.E. McCable, J. Li, E.J. Lepin, R. Remenyi, A.L. Koh, T. Olafsen, S.S. Gambhir, S. Weiss, A.M. Wu, Bioconjug. Chem. 20 (2009) 1474–1481.
[69] M.T. Fernández-Argüelles, J.M. Costa-Fernández, R. Pereiro, A. Sanz-Medel, Analyst 133 (2008) 444–447.
[70] Thermo Scientific: Pierce Protein Research Products, EDC (1-Ethyl-3-[3-dimethylaminopropyl]carbodiimide Hydrochloride, http://piercenet.com/Objects/View.cfm?type=ProductFamily&ID=02030312 (date accessed: May 13, 2010).
[71] K.E. Sapsford, T. Pons, I.L. Medintz, S. Higashiya, F.M. Brunel, P.E. Dawson, H. Mattoussi, J. Phys. Chem. C 111 (2007) 11528–11538.
[72] E.R. Goldman, I.L. Medintz, A. Hayhurst, G.P. Anderson, J.M. Mauro, B.L. Iverson, G. Georgiou, H. Mattoussi, Anal. Chim. Acta 534 (2005) 63–67.
[73] J.B. Delhanty, I.L. Medintz, T. Pons, F.M. Brunel, P.E. Dawson, H. Mattoussi, Bioconjug. Chem. 17 (2006) 920–927.
[74] D.E. Prasuhn, J.R. Deschamps, K. Susumu, M.H. Stewart, K. Boeneman, J.B. Blanco-Canosa, P.E. Dawson, I.L. Medintz, Small 6 (2010) 555–564.

[75] M.G. Sandros, D. Gao, C. Gokdemir, D.E. Benson, Chem. Commun. (2005) 2832–2834.
[76] I.L. Medintz, J.H. Konnert, A.R. Clapp, I. Stanish, M.E. Twigg, H. Mattousssi, J.M. Mauro, J.R. Deschamps, Proc. Natl. Acad. Sci. U.S.A. 121 (2004) 9612–9617.
[77] I.L. Medintz, L. Berti, T. Pons, A.F. Grimes, D.S. English, A. Alessandrini, P. Facci, H. Mattoussi, Nano Lett. 7 (2007) 1741–1748.
[78] L. Berti, P.S. D'Agostino, K. Boeneman, I.L. Medintz, Nano Res. 2 (2009) 121–129.
[79] R. Gill, I. Willner, I. Shweky, U. Banin, J. Phys. Chem. B 109 (2005) 23715–23719.
[80] H. Yao, Y. Zhang, F. Xiao, Z.Y. Xia, J. Rao, Angew. Chem. Int. Ed. 46 (2007) 4346–4349.
[81] E.R. Goldman, E.D. Balighian, H. Mattoussi, M.K. Kuno, J.M. Mauro, P.T. Tran, G.P. Anderson, J. Am. Chem. Soc. 124 (2002) 6378–6382.
[82] T. Pons, I.L. Medintz, X. Wang, D.S. English, H. Mattoussi, J. Am. Chem. Soc. 128 (2006) 15324–15331.
[83] T.Q. Vu, R. Maddipati, T.A. Blute, B.J. Nehilla, L. Nusblat, T.A. Desai, Nano Lett. 5 (2005) 603–607.
[84] D.S. Lidke, P. Nagy, R. Heintzmann, D.J. Arndt-Jovin, J.N. Post, H.E. Grecco, E.A. Jares-Erijman, T.M. Jovin, Nat. Biotechnol. 22 (2004) 198–203.
[85] S. Chattopadhaya, L.P. Tan, S.Q. Yao, Nat. Protocol 1 (2006) 2386–2398.
[86] K. Susumu, H.T. Uyeda, I.L. Medintz, H. Mattoussi, J. Biomed. Biotechnol. 2007 (2007) 90651.
[87] Z. Xia, Y. Xing, M.K. So, A.L. Koh, R. Sinclair, J. Rao, Anal. Chem. 80 (2008) 8649–8655.
[88] D.E. Prasuhn, J.B. Blanco-Canosa, G.J. Vora, J.B. Delehanty, K. Susumu, B.C. Mei, P.E. Dawson, I.L. Medintz, ACS Nano 4 (2010) 267–278.
[89] E.A. Jares-Erijman, T.M. Jovin, Nat. Biotechnol. 21 (2003) 1387–1395.
[90] A.R. Clapp, I.L. Medintz, H. Mattoussi, Chem. Phys. Chem. 7 (2006) 47–57.
[91] G. Allan, C. Delerue, Phys. Rev. B 75 (2007) 195311.
[92] C. Curutchet, A. Franceschetti, A. Zunger, G.D. Scholes, J. Phys. Chem. C 112 (2008) 13336–13341.
[93] A.R. Clapp, I.L. Medintz, J.M. Mauro, B.R. Fisher, M.G. Bawendi, H. Mattoussi, J. Am. Chem. Soc. 126 (2004) 301–310.
[94] T. Pons, I.L. Medintz, K.E. Sapsford, S. Higashiya, A.F. Grimes, D.S. English, H. Mattoussi, Nano Lett. 7 (2007) 3157–3164.
[95] I.L. Medintz, K.E. Sapsford, A.R. Clapp, T. Pons, S. Higashiya, J.T. Welch, H. Mattoussi, J. Phys. Chem. B 110 (2006) 10683–10690.
[96] T. Pons, I.L. Medintz, M. Sykora, H. Mattoussi, Phys. Rev. B 73 (2006) 245302.
[97] K. Beckner, A.L. Rogach, J. Feldmann, D.V. Talapin, J.M. Lupton, Appl. Phys. Lett. 95 (2009) 143101.
[98] I.H. Chung, K.T. Shimizu, M.G. Bawendi, Proc. Nat. Acad. Sci. U.S.A. 100 (2003) 405–408.
[99] A.R. Clapp, I.L. Medintz, B.R. Fisher, G.P. Anderson, H. Mattoussi, J. Am. Chem. Soc. 127 (2005) 1242–1250.
[100] A.L. Rogach, T.A. Klar, J.M. Lupton, A. Meijerink, J. Feldmann, J. Mater. Chem. 19 (2009) 1208–1221.
[101] L.J. Charbonnière, N. Hildebrandt, R.F. Ziessel, H.G. Löhmannsröben, J. Am. Chem. Soc. 128 (2006) 12800–12809.
[102] H. Härmä, T. Soukka, A. Shavel, N. Gaponik, H. Weller, Anal. Chim. Acta 604 (2007) 177–183.
[103] I.L. Medintz, J.R. Deschamps, Curr. Opin. Biotechnol. 17 (2006) 17–27.
[104] R. Freeman, L. Bahshi, T. Finder, R. Gill, I. Willner, Chem. Commun. (2009) 764–766.
[105] R. Freeman, R. Gill, I. Shweky, M. Kotler, U. Banin, I. Willner, Angew. Chem. Int. Ed. 48 (2009) 309–313.
[106] P.T. Snee, R.C. Somers, G. Nair, J.P. Zimmer, M.G. Bawendi, D.G. Nocera, J. Am. Chem. Soc. 128 (2006) 13320–13321.
[107] R. Nutiu, Y. Li, J. Am. Chem. Soc. 125 (2003) 4771–4778.
[108] G.I. Kim, K.W. Kim, M.K. Oh, Y.M. Sung, Nanotechnology 20 (2009) 175503.
[109] Z. Chen, G. Li, L. Zhang, J. Jiang, Z. Li, Z. Peng, L. Deng, Anal. Bioanal. Chem. 392 (2008) 1185–1188.
[110] C.Y. Zhang, L.W. Johnson, Anal. Chem. 81 (2009) 3051–3055.
[111] C.Y. Zhang, L.W. Johnson, Anal. Chem. 78 (2006) 5532–5537.
[112] C.Y. Zhang, L.W. Johnson, J. Am. Chem. Soc. 128 (2006) 5324–5325.
[113] C.Y. Zhang, L.W. Johnson, Anal. Chem. 79 (2007) 7775–7781.
[114] A.K.H. Cheng, H. Su, Y.A. Wang, H.Z. Yu, Anal. Chem. 81 (2009) 6130–6139.
[115] R. Freeman, Y. Li, R. Tel-Vered, E. Sharon, J. Elbaz, I. Willner, Analyst 134 (2009) 653–656.
[116] J. Liu, J.H. Lee, Y. Lu, Anal. Chem. 79 (2007) 4120–4125.
[117] R. Elghanian, J.J. Storhoff, R.C. Mucic, R.L. Letsinger, C.A. Mirkin, Science 277 (1997) 1078–1081.
[118] V. Bagalkot, L. Zhang, E. Levy-Nissenbaum, S. Jon, P.W. Kantoff, R. Langer, O.C. Farokhzad, Nano Lett. 7 (2007) 2070–3065.
[119] J.H. Kim, S. Chaudhary, M. Ozkan, Nanotechnology 18 (2007) 195105.
[120] N.C. Cady, A.D. Strickland, C.A. Batt, Mol. Cell. Probe 21 (2007) 116–124.
[121] A.K. Chen, M.A. Behlke, A. Tsourkas, Nucl. Acids Res. 35 (2007) e105.
[122] V.J. Bailey, H. Easwaran, Y. Zhang, E. Griffiths, S.A. Belinksy, J.G. Herman, S.B. Baylin, H.E. Carraway, T.H. Wang, Genome Res. 19 (2009) 1455–1461.
[123] W.R. Algar, U.J. Krull, Anal. Chim. Acta 581 (2007) 193–201.
[124] W.R. Algar, U.J. Krull, Langmuir 22 (2006) 11346–11352.
[125] D. Zhou, L. Ying, X. Hong, E.A. Hall, C. Abell, D. Klenerman, Langmuir 24 (2008) 1659–1664.
[126] C.S. Wu, J.M. Cupps, X. Fan, Nanotechnology 20 (2009) 305502.
[127] R. Bakalova, Z. Zhelev, H. Ohba, Y. Baba, J. Am. Chem. Soc. 127 (2005) 11328–11335.
[128] H. Peng, L. Zhang, T.H.M. Kjällman, C. Soeller, J. Travas-Sejdic, J. Am. Chem. Soc. 129 (2007) 3048–3049.
[129] J. Lee, Y. Choi, J. Kim, E. Park, R. Song, Chem. Phys. Chem. 10 (2009) 806–811.
[130] G. Jiang, A.S. Susha, A.A. Lutich, F.D. Stefani, J. Feldmann, A.L. Rogach, ACS Nano 3 (2009) 4127–4131.
[131] X. Li, J. Qian, L. Jiang, S. He, Appl. Phys. Lett. 94 (2009) 063111.
[132] Y.P. Ho, H.H. Chen, K.M. Leong, T.H. Wang, J. Control. Release 116 (2006) 83–89.
[133] H.H. Chen, Y.P. Ho, X. Jiang, H.Q. Mao, T.H. Wang, K.W. Leong, Mol. Ther. 16 (2008) 324–332.
[134] Y.P. Ho, H.H. Chen, K.W. Leong, T.H. Wang, Nanotechnology 20 (2009) 095103.
[135] H.H. Chen, Y.P. Ho, X. Jiang, H.Q. Mao, T.H. Wang, K.W. Leong, Nano Today 4 (2009) 125–134.
[136] M. Suzuki, Y. Husimi, H. Komatsu, K. Suzuki, K.T. Douglas, J. Am. Chem. Soc. 130 (2008) 5720–5725.
[137] E. Chang, J.S. Miller, J. Sun, W.W. Yu, V.L. Colvin, R. Drezek, J.L. West, Biochem. Biophys. Res. Commun. 334 (2005) 1317–1321.
[138] I.L. Medintz, A.R. Clapp, F.M. Brunel, T. Tiefenbrunn, H.T. Uyeda, E.L. Chang, J.R. Deschamps, P.E. Dawson, H. Mattoussi, Nat. Mater. 5 (2006) 581–589.
[139] L. Shi, V. De Paoli, N. Rosenzweig, Z. Rosenzweig, J. Am. Chem. Soc. 128 (2006) 10378–10379.
[140] K. Boeneman, B.C. Mei, A.M. Dennis, G. Bao, J.R. Deschamps, H. Mattoussi, I.L. Medintz, J. Am. Chem. Soc. 131 (2009) 3828–3829.
[141] Y.P. Kim, Y.H. Oh, E. Oh, S. Ko, M.K. Han, H.S. Kim, Anal. Chem. 80 (2008) 4634–4641.
[142] Y.P. Kim, Y.H. Oh, E. Oh, H.S. Kim, Biochip J. 1 (2007) 228–233.
[143] K.E. Sapsford, D. Farrell, S. Sun, A. Rasooly, H. Mattoussi, I.L. Medintz, Sens. Actuators B 139 (2009) 13–21.
[144] T.T. Nikiforov, J.M. Beechem, Anal. Biochem. 357 (2006) 68–76.
[145] R.C. Stringer, D. Hoehn, S.A. Grant, IEEE Sens. J 8 (2008) 295–300.
[146] X. Huang, L. Li, H. Qian, C. Dong, J. Ren, Angew. Chem. Int. Ed. 45 (2006) 5140–5143.
[147] H.Q. Wang, Y.Q. Li, J.H. Wang, Q. Xu, X.Q. Li, Y.D. Zhao, Anal. Chim. Acta 610 (2008) 68–73.
[148] L. Rowe, E. Dikici, S. Daunert, Anal. Chem. 81 (2009) 8662–8668.
[149] K.A. Cissell, S. Campbell, S.K. Deo, Anal. Bioanal. Chem. 391 (2008) 2577–2581.
[150] M.K. So, C. Xu, A.M. Loening, S.S. Gambhir, J. Rao, Nat. Biotechnol. 24 (2006) 339–343.
[151] Y. Xing, M.K. So, A.L. Koh, R. Sinclair, J. Rao, Biochem. Biophys. Res. Commun. 372 (2008) 388–394.
[152] D.E. Gómez, M. Califano, P. Mulvaney, Phys. Chem. Chem. Phys. 8 (2006) 4989–5011.
[153] A.P. de Silva, T.S. Moody, G.D. Wright, Analyst 134 (2009) 2385–2393.
[154] R.A. Bissell, A.P. de Silva, H.Q.N. Gunaratne, P.L.M. Lynch, G.E.M. Maguire, C.P. McCoy, K.R.A.S. Sandanayake, Top. Curr. Chem. 168 (1993) 223–264.
[155] R.A. Marcus, N. Sutin, Biochim. Biophys. Acta 811 (1985) 265–322.
[156] P.F. Barbara, T.J. Meyer, M.A. Ratner, J. Phys. Chem. 100 (1996) 13148–13168.
[157] P. Atkins, J. de Paula, Physical Chemistry, seventh ed., W.H. Freeman and Company, New York, 2002.
[158] M.J. Ruedas-Rama, E.A.H. Hall, Analyst 134 (2009) 159–169.
[159] M.J. Ruedas-Rama, E.A.H. Hall, Anal. Chem. 80 (2008) 8260–8268.
[160] D. Dorokhin, N. Tomczak, A.H. Velders, D.N. Reinhoudt, G.J. Vancso, J. Phys. Chem. C 113 (2009) 18676–18680.
[161] I.L. Medintz, T. Pons, S.A. Trammell, A.F. Grimes, D.S. English, J.B. Blanco-Canosa, P.E. Dawson, H. Mattoussi, J. Am. Chem. Soc. 130 (2008) 16745–16756.
[162] A. Boulesbaa, Z. Huang, D. Wu, T. Lian, J. Phys. Chem. C 114 (2010) 962–969.
[163] M.G. Sandros, V. Shete, D.E. Benson, Analyst 131 (2006) 229–235.
[164] M.J. Ruedas-Rama, E.A.H. Hall, Analyst 133 (2008) 1556–1566.
[165] M. Shim, C. Wang, P. Guyot-Sionnest, J. Phys. Chem. B 105 (2001) 2369–2373.
[166] I. Robel, M. Kuno, P.V. Kamat, J. Am. Chem. Soc. 129 (2007) 4136–4137.
[167] V.I. Klimov, Ch.J. Schwarz, D.W. McBranch, C.A. Leatherdale, M.G. Bawendi, Phys. Rev. B 60 (1999) R2177–R2180.
[168] E. Kuçur, W. Bücking, R. Giernoth, T. Nann, J. Phys. Chem. B 109 (2005) 20355–20360.
[169] E. Kuçur, J. Riegler, G.A. Urban, T. Nann, J. Chem. Phys. 119 (2003) 2333–2337.
[170] E. Kuçur, W. Bücking, S. Arenz, R. Giernoth, T. Nann, Chem. Phys. Chem. 7 (2006) 77–81.
[171] S.K. Poznyak, N.P. Osipovich, A. Shavel, D.V. Talapin, M. Gao, A. Eychmüller, N. Gaponik, J. Phys. Chem. B 109 (2005) 1094–1100.
[172] O.I. Mićić, A.J. Nozik, E. Lifshitz, T. Rajh, O.G. Poluektov, M.C. Thurnauer, J. Phys. Chem. B 106 (2002) 4390–4395.
[173] H. Levanon, K. Mobius, Annu. Rev. Biophys. Biomol. Struct. 26 (1997) 495–540.
[174] M.G. Sandros, D. Gao, D.E. Benson, J. Am. Chem. Soc. 127 (2005) 12198–12199.
[175] V.S. Shete, D.E. Benson, Biochemistry 48 (2009) 462–470.
[176] B.P. Aryal, D.E. Benson, J. Am. Chem. Soc. 128 (2006) 15986–15987.
[177] M.D. Swain, J. Octain, D.E. Benson, Bioconjug. Chem. 19 (2008) 2520–2526.
[178] I. Yildiz, M. Tomasulo, F.M. Raymo, Proc. Nat. Acad. Sci. U.S.A. 103 (2006) 11457–11460.
[179] I.L. Medintz, D. Farrell, K. Susumu, S.A. Trammell, J.R. Deschamps, F.M. Brunel, P.E. Dawson, H. Mattoussi, Anal. Chem. 81 (2009) 4831–4839.
[180] R. Gill, R. Freeman, J.P. Xu, I. Willner, S. Winograd, I. Shweky, U. Banin, J. Am. Chem. Soc. 128 (2006) 15376–15377.
[181] S.J. Clarke, C.A. Hollmann, Z. Zhang, D. Suffern, S.E. Bradforth, N.M. Dimitrijevic, W.G. Minarik, J.L. Nadeau, Nat. Mater. 5 (2006) 409–417.
[182] M.M. Richter, Chem. Rev. 104 (2004) 3003–3036.
[183] K.A. Fähnrich, M. Pravda, G.G. Guilbault, Talanta 54 (2001) 531–559.

[184] Z. Ding, B.M. Quinn, S.K. Haram, L.E. Pell, B.A. Korgel, A.J. Bard, Science 296 (2002) 1293–1297.
[185] N. Myung, Z. Ding, A.J. Bard, Nano Lett. 2 (2002) 1315–1319.
[186] N. Myung, Y. Bae, A.J. Bard, Nano Lett. 3 (2003) 1053–1055.
[187] N. Myung, X. Lu, K.P. Johnston, A.J. Bard, Nano Lett. 4 (2004) 183–185.
[188] Y. Bae, N. Myung, A.J. Bard, Nano Lett. 4 (2004) 1153–1161.
[189] Y. Bae, D.C. Lee, E.V. Rhogojina, D.C. Jurbergs, B.A. Korgel, A.J. Bard, Nanotechnology 17 (2006) 3791–3797.
[190] L. Shen, X. Cai, H. Qi, C. Zhang, J. Phys. Chem. C 111 (2007) 8172–8175.
[191] L. Sun, L. Bao, B.R. Hyun, A.C. Bartnik, Y.W. Zhong, J.C. Reed, D.W. Pang, H.D. Abruña, G.G. Malliaras, F.W. Wise, Nano Lett. 9 (2009) 789–793.
[192] S.K. Poznyak, D.V. Talapin, E.V. Shevchenko, H. Weller, Nano Lett. 4 (2004) 693–698.
[193] H. Jiang, H. Ju, Anal. Chem. 79 (2007) 6690–6696.
[194] H. Huang, J.J. Zhu, Biosens. Bioelectron. 25 (2009) 927–930.
[195] H. Huang, G. Jie, R. Cui, J.J. Zhu, Electrochem. Commun. 11 (2009) 816–818.
[196] G. Zou, H. Ju, Anal. Chem. 76 (2004) 6871–6876.
[197] H. Jiang, H. Ju, Chem. Commun. (2007) 404–406.
[198] Y. Wang, J. Lu, L. Tang, H. Chang, J. Li, Anal. Chem. 81 (2009) 9710–9715.
[199] S.N. Ding, J.J. Xu, H.Y. Chen, Chem. Commun. (2006) 3631–3633.
[200] X.F. Wang, Y. Zhou, J.J. Xu, H.Y. Chen, Adv. Funct. Mater. 19 (2009) 1444–1450.
[201] G. Jie, J. Zhang, D. Wang, C. Cheng, H.Y. Chen, J.J. Zhu, Anal. Chem. 80 (2008) 4033–4039.
[202] G. Jie, L. Li, C. Chen, J. Xuan, J.J. Zhu, Biosens. Bioelectron. 24 (2009) 3352–3358.
[203] G. Jie, H. Huang, X. Sun, J.J. Zhu, Biosens. Bioelectron. 23 (2008) 1896–1899.
[204] G. Jie, B. Liu, H. Pan, J.J. Zhu, H.Y. Chen, Anal. Chem. 79 (2007) 5574–5581.
[205] Y. Shan, J.J. Xu, H.Y. Chen, Chem. Commun. (2009) 905–907.
[206] X. Liu, L. Cheng, J. Lei, H. Ju, Analyst 133 (2008) 1161–1163.
[207] X. Liu, H. Ju, Anal. Chem. 80 (2008) 5377–5382.
[208] W.R. Algar, U.J. Krull, Langmuir 25 (2009) 633–638.
[209] W.R. Algar, U.J. Krull, Anal. Chem. 81 (2009) 4113–4120.
[210] W.R. Algar, U.J. Krull, Anal. Chem. 82 (2010) 400–405.
[211] W.R. Algar, U.J. Krull, Langmuir 26 (2010) 6041–6047.
[212] H.T. Beier, G.L. Coté, K.E. Meissner, Annu. Biomed. Eng. 37 (2009) 1974–1983.
[213] R. Robelek, L. Niu, E.L. Schmid, W. Knoll, Anal. Chem. 76 (2004) 6160–6165.
[214] K.T. Shimizu, W.K. Woo, B.R. Fisher, H.J. Eisler, M.G. Bawendi, Phys. Rev. Lett. 89 (2002) 117401.
[215] A. Kinkhabwala, Z. Yu, S. Fan, Y. Avlasevich, K. Müllen, W.E. Moerner, Nat. Photon 3 (2009) 654–657.
[216] N. Ganesh, W. Zhang, P.C. Mathias, E. Chow, J.A.N.T. Soares, V. Malyarchuk, A.D. Smith, B.T. Cunningham, Nat. Nanotechnol. 2 (2007) 515–520.
[217] R.S. Dibbell, G.R. Soja, R.M. Hoth, D.F. Watson, Langmuir 23 (2007) 3432–3439.
[218] P.J. Cameron, X. Zhong, W. Knoll, J. Phys. Chem. C 113 (2009) 6003–6008.
[219] S. Aoyagi, M. Inoue, Appl. Surf. Sci. 256 (2009) 995–997.
[220] O.V. Vassiltsova, S.K. Panda, Z. Zhao, M.A. Carpenter, M.A. Petrukhina, Dalton Trans. (2009) 9426–9432.
[221] V. Pardo-Yissar, E. Katz, J. Wasserman, I. Willner, J. Am. Chem. Soc. 125 (2003) 622–623.
[222] M.T. Zin, A.M. Munro, M. Gungormus, N.Y. Wang, H. Ma, C. Tamerler, D.S. Ginger, M. Sarikaya, A.K.Y. Jen, J. Mater. Chem. 17 (2007) 866–872.
[223] D. Baş, I.H. Boyaci, Electroanalysis 21 (2009) 1829–1834.
[224] A. Gole, N.R. Jana, S.T. Selvan, J.Y. Ying, Langmuir 24 (2008) 8181–8186.
[225] C.A. Constantine, K.M. Gattás-Asfura, S.V. Mello, G. Crespo, V. Rastogi, T.C. Cheng, J.J. DeFrank, R.M. Leblanc, Langmuir 19 (2003) 9863–9867.
[226] A.M. Coto-García, M.T. Fernández-Argüelles, J.M. Costa-Fernández, A. Sanz-Medel, Chem. Commun. (2009) 5454–5456.
[227] K.M. Gattás-Asfura, Y. Zheng, M. Micic, M.J. Snedaker, X. Ji, G. Sui, J. Orbulescu, F.M. Andreopoulos, S.M. Pham, C. Wang, R.M. Leblanc, J. Phys. Chem. B 107 (2003) 10464–10469.
[228] W. Wu, T. Zhou, J. Shen, S. Zhou, Chem. Commun. (2009) 4390–4392.
[229] R. Gill, F. Patolsky, E. Katz, I. Willner, Angew. Chem. Int. Ed. 44 (2005) 4554–4557.
[230] W.R. Algar, U.J. Krull, Langmuir 24 (2008) 5514–5520.
[231] P.T. Tran, E.R. Goldman, G.P. Anderson, J.M. Mauro, H. Mattoussi, Phys. Stat. Sol. B 229 (2002) 427–432.
[232] K.E. Sapsford, I.L. Medintz, J.P. Golden, J.R. Deschamps, H.T. Uyeda, H. Mattoussi, Langmuir 20 (2004) 7720–7728.
[233] W.R. Algar, U.J. Krull, unpublished data.
[234] W.R. Algar, U.J. Krull, In: A. Alexandrou, J. Cheon, H. Mattoussi, V. Rotello (Eds.), Biological Imaging and Sensing Using Nanoparticle Assemblies, Mater. Res. Soc. Symp. Proc., vol. 1241E, Warrendale, PA, 2010, paper no.1241-XX09-04.
[235] C.Y. Zhang, J. Hu, Anal. Chem. 82 (2010) 1921–1927.
[236] C.L. Feng, X.H. Zhong, M. Steinhart, A.M. Caminade, J.P. Majoral, W. Knoll, Small 4 (2008) 566–571.
[237] H. Qi, L. Wang, K.W. Wong, Z. Du, Appl. Phys. Lett. 94 (2009) 143902.
[238] I.L. Medintz, A.R. Clapp, J.S. Melinger, J.R. Deschamps, H. Mattoussi, Adv. Mater. 17 (2005) 2450–2455.
[239] L. Cao, J. Ye, L. Tong, B. Tang, Chem. Eur. J. 14 (2008) 9633–9640.
[240] A.R. Clapp, I.L. Medintz, H.T. Uyeda, B.R. Fisher, E.R. Goldman, M.G. Bawendi, H. Mattoussi, J. Am. Chem. Soc. 127 (2005) 18212–18221.